Kū Hou Kuapā: Increase of water exchange rates and changes in microbial source tracking markers resulting from restoration regimes at He‘eia Fishpond

A THESIS SUBMITTED TO THE GRADUATE DIVISION OF THE UNIVERSITY OF HAWAI‘I AT MĀNOA IN PARTIAL FULFILLMENT OF THE REQUIREMENTS FOR THE DEGREE OF

MASTER OF SCIENCE

IN

OCEANOGRAPHY

July 2018

By
Paula Moehlenkamp

Thesis Committee:

Margaret McManus and Rosanna Alegado, Co-Chairperson

Craig Nelson,

Brian Glazer

Keywords: He‘eia Fishpond; community restoration; conservation ecology

ACKNOWLEDGEMENTS

I would like to express my utmost gratitude and thanks to Dr. Margaret McManus and Dr. Rosie Alegado, for their unwavering support, guidance, and enthusiasm over the past two years. Their insights were invaluable for the growth and success of this research and their example as hard-working oceanographers, putting in many extra hours out of love for science, has impacted and inspired me tremendously. They have become great role models to me that I will often and gladly think of as I continue to grow as a young scientist. Thank you so much for being such tremendous mentors, encouraging my research and for allowing me to grow as a research scientist.

I also would like to thank the members of my committee, Dr. Craig Nelson and Dr. Brian Glazer, for their support and feedback throughout this research project. Their comments and suggestions have greatly improved my research and each played a significant role in seeing this work come to fruition. I would also like to express my sincere appreciation to Dr. Kathleen Ruttenberg for the provision of Sontek Argonaut current meters that were invaluable for our physical measurements.

This project would not have been possible without the support and collaboration Paepae o He‘eia, who have been incredibly welcoming and invaluable in informing me about their work at the fishpond. Special thanks to Keli‘i Kotubetey for always being available and helping me to develop a better understanding of the fishpond environment through many, enjoyable conversations. To work on a project with direct implications for the restoration of this culturally and economically significant site, felt very meaningful to me and I could not have wished for a more beautiful and friendlier environment to work in.

I gratefully acknowledge all the members of the Alegado, Nelson and McManus lab: Charles Aka Beebe, who has been an extraordinary help with field work, Mirielle Lopez-Gusman and Kristina Remple, who have been invaluable with their help in qPCR analysis in the laboratory, and Christina Comfort, Conor Jerolmon and Gordon Walker, for their assistance with field work and data analysis. I would also like to acknowledge the many Oceanography friends and peers that accompanied me to the fishpond and assisted me with field work: Nalani Olguin, Camilla

Tognacchini, Kate Feloy, Carleigh Vollbrecht, Angeles Gallego, Lisa Hahn-Woernle, No‘eau Machado, Juno Fitzpatrick, Seth Travis, Alma Trujillo. I am very grateful to have had this extraordinary support.

This research was sponsored by the University of Hawaii Sea Grant College Program and the Hawai‘i Department of Health.

ABSTRACT

Anthropogenic activities have changed island ecosystems throughout history. Hawai‘i’s natural environment has been dramatically altered by land use change, urbanization, pollution, and the introduction of invasive species causing a demise of traditional Hawaiian fishponds across the state over the last century. He‘eia fishpond is currently being restored and provides- embedded between land and sea- a unique opportunity to examine how historical land use change has altered the functions of coastal habitats and how restoration can help to maintain and improve the integrity of coastal ecosystems in the face of rapid global change.

He‘eia fishpond is an example of a traditional Hawaiian aquaculture system at the terminus of He‘eia ahupua‘a on the windward site of O‘ahu, Hawai‘i. It is a natural embayment that is enclosed by a constructed wall (kuapā) with sluice gates (mākāhā) facilitating water exchange crucial for fish survival. This study examines how major restoration regimes, as the removal of invasive mangroves, and the reconstruction of a 50 m section of the kuapā known as “Ocean Break”, impacted water exchange rates, residence times, salinity distribution, as well as abundance of microbial source tracking markers.

Our study revealed that He‘eia fishpond’s physical environment is largely tidally driven during baseline (non-storm) conditions with wind forcing and river flux being secondary drivers. Post-restoration, two (OM1/*Mākāhā Nui*, *Kaho‘okele* (former OB)) of six mākāhā accounted for over 80% of relative flux together, making the northeastern region of the fishpond the dominant flow pathway of water into and out of the fishpond. The repair of Ocean Break increased water exchange rates ~5% during spring tide and ~16% during neap tide and similarly decreased minimum water residence time in the fishpond from 38 hours to 32 hours and maximum residence time from 102 hours to 64 hours. Salinity distribution displayed a spatial gradient across the fishpond with higher salinities on the ocean side of the fishpond and lower salinities towards the fresh water dominated site. Comparison of pre- vs. post-restoration salinity revealed significantly lower average salinities post-restoration, an indication for increased fresh water flux due to mangrove removal around the northern fishpond periphery. Spatial distribution of microbial source tracking markers was inversely correlated with salinity. Despite decreased

residence times, average abundance of *Enterococcus* and *Bacteroidales* did not significantly change after restoration efforts. As these microbes are introduced through freshwater from terrigenous runoff, the increase in fresh water flushing post-restoration presents a mechanism increasing overall abundance, hence counteracting the positive impact increased exchange rates may have on water quality. However, average abundance of *Fusobacteria*, a biomarker specific to fecal contamination from cattle egrets living at the fishpond, decreased significantly after restoration. The source of bird microbial contamination lies in the fishpond and is less dependent on terrigenous freshwater input suggesting that increased flushing affected bird biomarker abundance. Taken together microbial source tracking is a promising avenue to pursue further in understanding how restoration and changes in circulation relate to microbiological water quality assessments.

Repairing the wall restored the fishpond to its traditional nature: A loko kuapā - a seashore fishpond with an artificial stone wall enclosing the system during all tidal states and sluice gates facilitating rigorous water exchange in particular in the eastern portion of the fishpond. To avoid events with mass fish mortality in the future, we recommend moving fish pens strategically to the eastern region of the fishpond (close to *Kaho'okele* and OM1), which exhibit the highest flushing rates with favorable conditions for fish to thrive. This study clearly demonstrates the positive impact restoration regimes have had on water flushing and water quality parameters encouraging the prospect of revitalizing this culturally and economically significant site for sustainable aquaculture in the future.

TABLE OF CONTENTS

LIST OF TABLES

LIST OF FIGURES

1. INTRODUCTION

1.1. Traditional Hawaiian food sustainability and subsistence practices

Ahupua‘a, an ancient Hawaiian land division spanning from mountain ridges to the ocean and reefs [1], typically coincided with watershed boundaries and provided a physical, socioeconomic, and cultural structure wherein ancient Hawaiians, practiced sustainable resource use and management [2,3]. Inhabiting a geographically isolated space in the center of the Pacific, Hawaiians viewed themselves as an integral part of nature and understood that “mālama ka ‘āina”, the harmonization of human health with the health of the land, through protection and care of the natural resources, was necessary to sustain themselves and future generations [1,3]. By taking care of the land, Hawaiian culture was not only able to survive but thrive in such a remote space with limited resources [2,3]. Hence, the concept of sustainability stands at the core of Hawaiian cultural and spiritual identity.

Nearshore fishponds (loko i‘a kuapā) like He‘eia were an integral part of the ahupua’a land use system and presented a crucial source of protein to the Hawaiian community when shoreline fishing was not feasible or did not yield sufficient supply [4–6]. With the construction of walled fishponds, Hawaiians were able to complement and enhance the natural productivity that surrounded them [7]: Located adjacent to the sea, loko i‘a kuapā fishponds were characterized by a mixture of fresh and ocean water. The combination of brackish water with nutrients and other organic materials from the runoff of stream water that had circulated in lo‘i (upstream flooded agroecosystems based on taro), shallow water depth, maximum sunlight exposure, and circulation from tides and stream flows, fostered a extremely productive, estuary-type environment and an ideal nursery ground for herbivorous fish [7]. This autarchic feeding system based on fish protein through natural algae (Hawaiian: limu), provided a particularly efficient and sustainable food-chain relationship [6].

Mullet (Hawaiian: awa) and milkfish (Hawaiian: ‘ama‘ama) were two of the most common species raised by Hawaiians in fishponds, both of which are now depleted in Hawai‘i because of land use change and the loss of habitats [7]. Before the arrival of Western influence in 1778, estimates suggest a total production of 900,000 kg fish per year from 360 Hawaiian fishponds

across the islands [8]. However, by 1977 only 28 fishponds were still in production and continuing this declining trend by 1985 only 7 fishponds were in commercial or subsidence use [6].

1.2. Land use change in Hawai‘i

The dramatic decline in the number of Hawaiian fishponds has largely been attributed to a combination of social, economic, and natural influences: Changing lifestyles and economics, transfer from a traditional ahupua‘a management system to a plantation style, which was much more prone to erosion, consequently leading to large scale siltation of these ecosystems, urbanization and pollution, the introduction of invasive species, as well as natural influences as storms, floods, tsunamis and lava flows, lead to the deterioration of Hawaiian fishponds all over the state [6]. The red mangrove *(Rhizophora mangle)* is the most prevalent species, growing thick forests with tangles of aerial roots. In their native environment, mangroves are highly appreciated for the ecosystem services they provide throughout the tropics. The many positive ecosystem services mangroves provide, include shoreline protection and sediment stabilization [9], litterfall subsidy [10] and provision of nursery grounds [11]. By modifying their environment strongly, mangroves have cascading effects for resident biota, therefore acting as important ecosystem engineers when native [9]. However, in Hawai‘i, mangroves also have a variety of negative ecological and economic impacts that need to be considered. Known negative impacts include the transformation of nearshore sandy habitat into heavily vegetated areas with decreased water velocity, high sedimentation rates, and anoxic sediments through bacterial decomposition of mangrove leaf detritus [12,13].

1.3. He‘eia Fishpond: History, restoration and management

He‘eia fishpond is an example of a traditional Hawaiian aquaculture system located on the windward site of O‘ahu, Hawai‘i (21°26′10.74″ N, 157°48′28.05″W) that has been altered profoundly through human interaction [4,5,14,15]. Hawaiian fishponds are one of the most ancient and sustainable aquaculture systems in the world and hold important cultural value [4–6,14]. Thought to be the birthplace of mariculture-seawater farming, traditional Hawaiian fishponds have been dated back to 1500-1800 years before present and described as significant and successful aquaculture with “remarkable sophistication in terms of their diversity, distinctive

management and sheer extend of development" [6]. He‘eia fishpond is part of He‘eia ahupua‘a, a traditional resource management unit comprising the Ha‘ikū and Ioleka‘a watersheds and extending out to *Moku o Lo‘e.*

Recently, there has been an effort to restore many of the existing fishponds throughout Hawai'i [7]. In 2013, there were almost 100 fishponds in the state of Hawai‘i that were undergoing restoration [8]. Among them, He‘eia Fishpond is one of the most studied examples of fishpond restoration efforts. Restoration regimes at the fishpond are managed by the nonprofit organization Paepae o He‘eia, who strive to restore the fishpond to its non-impacted ecological state and resume commercial or community-based fishing. By linking traditional knowledge and contemporary management practices, Paepae o He‘eia hopes to foster cultural sustainability and restore and maintain a thriving fishpond for the community. Their mission is "to implement values and concepts from the model of a traditional fishpond to provide physical, intellectual, and spiritual sustenance for our community" (www.paepaeoheeia.org). More recently, in part because of the ongoing concerted efforts of community organizations like Paepae o He‘eia, the coastal area of He‘eia was designated as National Estuarine Research Reserve (NERR) in January 2017 to advance research and protection of the He‘eia ahupua‘a by integrating the traditional Hawaiian ecosystem management approach with contemporary estuarine management practices [8].

A main focus of Paepae o He'eia's restoration effort have been the removal of invasive mangroves from the fishpond periphery. Mangroves were introduced to Hawai‘i in 1902 and have since overgrown many coastal areas [8]. Mangroves were introduced to the ahupua‘a of He‘eia around 1922 to control runoff from upstream agriculture and stabilize sediments [15,16]. Thriving in the Hawaiian environment, mangroves spread quickly, forming a large area of dense mangrove forest around the mouth of He‘eia stream eventually expanding past the stream and overgrowing the fishpond wall completely.

For a confined, shallow water environment such as He‘eia Fishpond these effects have important implications as consistent aeration and circulation is crucial to maintain stable oxygen levels for fish survival [17]. Additionally, as mangroves grow within the wall, their many aerial roots

loosen the rocks and coral destroying the wall's structural integrity [17]. For these reasons, the removal of invasive mangroves presents an important management practice at He‘eia fishpond. Since 2001, Paepae o He‘eia have removed mangrove along the pond periphery clearing the side of the kuapā bordering the ocean entirely (reflected in a mangrove removal chronological sequence, Figure 1). Paepae o He‘eia started clear-cutting the mangrove comprising "Mangrove Island" (Figure 1), home to a 2000 to 3000 cattle egret *(Bubulcus ibis)* colony in 2017. Egret fecal matter presents a potential source of phosphorous and other nutrients, as well as microbial contamination to the region.

Another step in the restoration process involved the reconstruction of a section of the wall (kuapā) that had been broken during a major flood in 1965. After the flood, the 56 m long gap in the kuapā was confined with a provisional elbow wall using concrete blocks, which retained water within the fishpond. However, the provisional elbow wall -also referred to as "Ocean Break"- was not as high as the remaining kuapā allowing water to overflow this section of the wall during certain high tides. When the water level in Kāne‘ohe Bay exceeded the concrete wall height, Ocean Break facilitated large amounts of water exchange during high tidal stages. In 2015, Ocean Break was rebuilt to the same height as the existing wall, using original kuapā materials – pohaku pele (volcanic rock) and ko‘a (coral). In addition, a new mākāhā channel named Kaho‘okele was installed. The present study examines how the removal of invasive mangroves around the northern fishpond periphery from 2014-2017 and the repair of Ocean Break in 2015 impacted various aspects of the fishpond and presents a comparison of pre- vs. post-restoration ecosystem dynamics.

1.4. Research Goals

Embedded between land and sea, He‘eia Fishpond acts as a powerful natural laboratory providing the unique opportunity to examine how historical land use change has altered the functions of coastal habitats and how restoration can help to maintain and improve the integrity of these coastal ocean ecosystems in the face of rapid global change. A variety of studies have been conducted to characterize the physical and geochemical environment of He‘eia Fishpond. A recent study by McCoy et al. [17] examined large scale climatic effects on He‘eia Fishpond and found a correlation between El Niño warming events with slackening trade winds and periods of

high fish mortality experienced in 2009. The study proposed that the combination of a lack of trade wind-driven surface water mixing and enhanced surface heating as well as stratification of the water column lead to hypoxic stress on fish populations [17] rendering need to understand flushing patterns in He‘eia Fishpond. If fish pens would be moved to areas that are well circulated and under constant aeration, fish mortality events could be prevented in the future [17]. Measurement of physical characteristics of He‘eia Fishpond before restoration revealed that ~90% of fishpond water exchange occurred in the northeast corner of the fishpond via Ocean Break (~80%) and Ocean Mākāhā 1 (~10%) suggesting that the eastern half of the fishpond was better mixed and less stratified than the western side of the fishpond [18,19]. Water volume flux rates were found to be largely tidally driven, with flux exhibiting the greatest volume exchange at mid tides [18, 19]. Volume estimates before restoration revealed that ~77% of total fishpond water was exchanged during spring tide, while neap tide exchanged ~42% of water [19]. River mākāhā in the northwest corner were found to be the only direct source for freshwater from He'eia Stream and accounted for the only region in the fishpond with mean salinity routinely less than 20 ppt [18,19].

The present study was aimed at understanding the direct impact of restoration regimes on the fishpond circulation dynamics such as the dominant flow pathways of water into and out of the fishpond, exchange rates, residence time and salinity distribution. In addition, we investigated the link between physical characteristics of the fishpond and microbial biomarker distribution, which were used as an indication for water quality. A central question in maintaining an ecologically balanced and productive fishpond is the potential for human and animal health impacts from microbial contamination, and microbial source tracking methods present a way to quantify fecal indicator bacteria from human or avian feces to assess water quality [20,21].

The specific goals of the present study were to:

(i) Evaluate how kuapā infrastructure repair (the closure of Ocean Break with the incorporation of *Kaho‘okele*), as well as the continuation of invasive mangrove clearance around the fishpond periphery, have affected relative water flux at the mākāhā, fishpond water exchange rates and residence time.

(ii) Understand the impact of changing circulation dynamics on salinity distribution and abundance of microbial source tracking markers within the fishpond.

To address these research goals, we reevaluated water flux in 2018 by quantifying the volume of water (m^3 s^{-1}) moving into and out of each mākāhā with current meters and fishpond water exchange and residence time with *in situ* water level loggers as well as bathymetry data. In addition, we recalculated rating curves that determine flow into and out of He'eia fishpond for each of the mākāhā from the flux data collected. The physical environment post-restoration was then compared with pre-restoration data published in Timmerman et al. [19]. Salinity measurements from pre and post-restoration work were analyzed as an indicator of fishpond circulation, mixing and stratification. Finally, genomic DNA extracted from discrete water samples were utilized for microbial source tracking of fecal indicator bacteria. Together, this comprehensive data set allowed us to draw a linkage between restoration efforts and changing fishpond circulation as well as water quality dynamics.

2. MATERIALS AND METHODS

2.1. Study site

The ahupuaʻa of Heʻeia is located on the windward side of the island of Oʻahu, Hawaiʻi, within the ahupuaʻa of Heʻeia adjacent to Kāneʻohe Bay (Figure 2). Heʻeia ahupuaʻa extends across 11,500 km^2 (2,843 acres) and comprises roughly 10% of the Kāneʻohe Bay Watershed (23,500 acres). Heʻeia Stream originates as the Haʻikū Stream near the ridgeline of the Koʻolau Mountains and converges with the ʻIolekaʻa Stream before entering the Hoi wetlands dominated by non-native and invasive plant species. Historically, upon exiting the wetlands, Heʻeia Stream was diverted to the south through auwai (irrigation ditch) before flowing into Heʻeia Loko Iʻa (fishpond) and Kāneʻohe Bay (Figure 3).

Located at the terminus of the Heʻeia ahupuaʻa, Heʻeia Fishpond is an approximately 88-acre (0.356 km^2) embayment bordered by Kāneʻohe Bay on the ocean side and mangrove forest along the terrestrial periphery privately owned by Kamehameha Schools. Built approximately 600-800 years ago by the residents of the watershed [22] on the Malaukaʻa fringing reef Heʻeia Fishpond is a *loko iʻa kuapā*-style fishpond with the pond periphery being entirely enclosed by a constructed wall (kuapā). A typical feature of Heʻeia Fishpond is the kuapā, which encloses the fishpond for approximately 2.5 km. Kuapā are built from two parallel volcanic rock walls filled with coral rock rubble (Figure 4) periodically broken up by mākāhā (sluice gates), which facilitate water exchange into and out of the fishpond. The kuapā fulfills multiple functions: It regulates freshwater inflow to mākāha, protects the fishpond from waves and presents a partial barrier to wind, and it slows down water flux into and out of the fishpond and ensures that a minimum volume of water remains in the fishpond at all times, even at extremely low tides. In addition, the kuapā allows stewards to close mākāhā to regulate freshwater and/or seawater influx/outflow. Water geochemistry within Heʻeia fishpond is characterized by influx of distinct water masses: freshwater from Heʻeia stream that varies depending on the amount of precipitation, submarine groundwater discharge [23], and seawater from Kāneʻohe Bay that fluctuates with the tidal cycle. Four saltwater mākāhā allow bi-directional flow that is largely mediated by the semi-diurnal tidal cycle in Kāneʻohe Bay. At flood tide ocean water flows into pond, while at ebb tide flow direction reverses and water is advected out of the pond.

Seven mākāhā connect the fishpond to exterior water sources and regulate stream and seawater exchange with the fishpond (Figure 5-6).

Mākāhā names used in this study were adopted from Paepae o He‘eia, the Native Hawaiian stewards of the fishpond (paepaeoheeia.org) as well as previous studies (Nā Kilo Honua o He‘eia, http://www.nakilohonuaoheeia.org and Young (2011), [18]), Figure 6, Table 1. The mākāhā dominated by saltwater and closest to the mouth of He’eia Stream (*Ka Hoa Lāhui* /Triple Mākāhā, hereafter TM) is comprised of three channels of similar size *Ke‘alohi*, *Ko‘a Mano*, and *Kapapa* (from North to South). For the purpose of this study, we treated TM as a single mākāhā and for quantification of water budget, we measured flow measurements at the northern most mākāhā channel (*Kealohi)* and multiplied by three. To the south of TM, *Mākāhā Nui/*Ocean Mākāhā 1 (hereafter OM1) has the largest channel in width. The easternmost mākāhā, *Kaho‘okele*/Ocean Break (hereafter OB (pre-restoration) and *Kaho‘okele* (post-restoration)) was reconstructed over the course of this study. Prior to restoration, a 56 m section of the wall was destroyed during the 1965 Keapuka flood [19]. From 1965-2015, water exchange in this area of the fishpond was mediated by a 1 m deep elbow wall composed of concrete cylinder blocks. The mākāhā farthest from He‘eia stream is *Hīhīmanu*/Ocean Mākāhā 2 (hereafter OM2).

Historically, three freshwater mākāhā provided conduits for He‘eia Stream water to flow into the fishpond. Flux through the most seaward mākāhā along the He‘eia Stream, Wai 1/River Mākāhā 3 (hereafter RM3) is affected by tidal activity and is the only freshwater mākāhā that allows bi-directional water flow into and out of the fishpond [18]. Located ~100 m upstream of Wai 1, Wai 2/River Mākāhā 2 (hereafter RM2) has unidirectional flow into the fishpond with little tidal influence. The most upstream mākāhā and at the highest elevation, was destroyed during the 1965 Keapuka flood and has not yet been restored. As a result, this most upstream mākāhā (River Mākāhā, hereafter RM1) does not have a constructed flow channel, but is rather characterized by a diffusive flow region [18]; thus, measurements with current meters at RM1 were not feasible. Water flux through the three freshwater mākāhā varies with seasonal rainfall during episodic storm events with high rainfall, strong freshwater influx can have pronounced effects on the fishpond system [18].

An additional function of the mākāhā system is to restrict flow thereby causing a delay in fishpond tidal signal [18] when referenced to the tidal signal recorded by *Moku o Lo'e* tide gauge at HIMB. The limited flow through the mākāha cause the fishpond to drain more slowly during ebb tide, thus, ensuring a minimum water volume at all times, including extremely low tides. All modern mākāhā channels have concrete floors that are slightly higher than the natural bottom of the fishpond, except for OB, which has a lower concrete floor. Like the kuapā, the vertical wall enclosing the mākāhā channel is composed of basalt and coral rubble. The contemporary mākāhā gates are a semi-permeable barrier fence or grid constructed from wood or plastic (Figure 7); spaced evenly to allow water and fish smaller than the space between wooden grid to enter and exit from the fishpond freely.

2.2. Characterization of fishpond water flux, volume, residence time and salinity post-restoration

2.2.1. Data collection with *in situ* instrumentation

To assess the effect of restoration regimes on water volume flux, fishpond volume and residence time, *in situ* instruments were deployed throughout He'eia Fishpond to obtain data on currents, changes in water level due to tidal activity, water temperature and salinity. Data associated with hydro-meteorological conditions, including tidal height, rainfall as well as wind direction and speed, were considered in order to assess influence of these parameters on water volume flux, fishpond volume, residence time and water quality in He'eia Fishpond. An overview of *in situ* instrumentation, data type, sampling frequencies, location and rationale for each measurement is presented in Table 2.

2.2.2. Regional meteorological and tidal data

Rainfall data for this study was obtained from National Oceanic and Atmospheric Administration's (NOAA) Luluku (HI15) rain gauge station (http://www.prh.noaa.gov/hnl/hydro/hydronet/hydronet-data.php, Figure 8) as Luluku Station has previously shown to be a good indicator for storm events within southern Kāne'ohe Bay [19,24]. Luluku Station HYDRONET rain gage readings were taken every 15 minutes. The rainfall data provided the criteria for comparing weather conditions between different sample

events. Rainfall data were recorded in daily rainfall (cm 24 hrs^{-1}) and cumulative rainfall over 4 days (cm 96 hrs^{-1}) for each sampling event. To estimate stream discharge into He‘eia Fishpond, stream flow data (mean m^3 s^{-1} 24 hrs^{-1}) was obtained from Ha‘iku Stream, primary freshwater source to He‘eia Stream [18], from USGS Ha‘iku Stream discharge station (Station #16275000) upstream of He‘eia Fishpond. Stream flow data can be accessed on the USGS water data website (http://waterdata.usgs.gov).

Wind direction and magnitude were downloaded from Hawaii Institute of Marine Biology (HIMB) automatic weather station (AWS) *Moku o Lo‘e* (Figure 8). This weather station is located on the southeastern edge of Moku o Lo‘e in Kāne‘ohe Bay approximately 1.5 km from He‘eia Fishpond. Instruments are mounted on the roof of the HIMB Coral Reef Ecology Laboratory approximately 5 m above sea level. Sensors include an Eppley 295-385 nm ultraviolet (UV) radiometer, a LiCor 200SZ Pyranometer, and a LiCor Quantameter (400-700 nm). An accompanying sea level gauge and water temperature probe is located less than 10 m offshore of the weather station at a shallow depth of approximately 1 m. The weather station records and transmits hourly measurements of air and water temperature (°F), wind speed (m.p.h.), direction (°), precipitation (in.), and irradiance (W/m^2). Data and plots are available from the Pacific Island Ocean Observing System (PacIOOS) website (http://www.pacioos.hawaii.edu/weather/obs-mokuoloe/). Wind data from the HIMB weather station is in close proximity to He‘eia fishpond and therefore provides a context when analyzing the influence of wind and tide changes on the fishpond.

Kāne‘ohe Bay has mixed semidiurnal tides, meaning there are two high tides and two low tides of unequal height within 24 hours. The influence of tidal activity from Kāne‘ohe Bay is not consistent between tides at He‘eia Fishpond. Semidiurnal tides are of differing magnitude, thus the flow rate of marine water into the fishpond varies over time. Tidal data for the region was utilized from *Moku o Lo‘e* at HIMB (http://tides.mobilegeographics.com/locations/3854.html). The HIMB *Moku o Lo‘e* tide gauge data allowed us to assess how much tidal amplitudes changed between pre- vs. post-restoration.

2.2.3. Multiparameter sonde measurements

Along with discrete water sample collection, data from a YSI Professional Plus (ProPlus) multi-parameter water quality sonde (YSI Xylem Brand, Yellow Springs, Ohio) were used to produce maps of salinity. Horizontal and vertical gradients in the salinity indicate the extent of freshwater intrusion in the fishpond as well as the amount of mixing. The 2017 sampling grid was comprised of 11 sampling locations within the fishpond (Figure 9, Table 3), 6 sampling locations at the mākāhā (M01−M06) and one end member location in He‘eia Stream and Kāne‘ohe Bay (E01 and E02). The 2014 sampling grid was comprised of 10 sampling locations within the fishpond (P1−P10) for the YSI measurements. To minimize the disturbance of the water column prior to measurements, sampling sites were approached against prevailing currents and winds. At each location, two measurements were taken with the water column profiling instrumentation: a surface measurement approximately 5-10 cm below the water surface and a bottom measurement 5-10 cm above the benthos. The YSI multi-parameter water quality sonde was held in place for 2-3 minutes until values normalized. For the present study, only salinity data were analyzed from the YSI measurements.

2.2.4. Sontek Argonaut SW flow meter

Current meters were deployed in each mākāhā to evaluate the dominant flow paths of water into and out of the fishpond. Sontek Argonaut flow SW (SonTek, San Diego, CA) meters measure water velocity (m s^{-1}) current direction (in degrees) in two dimensions via the acoustic Doppler method. Water level (m) was measured with a third vertical acoustic beam. Current meters were deployed over the course of 7 days at each of the 6 sluice gates that provide channelized flow. Water flux data allows for an evaluation of the relative importance of water volume flux at each mākāhā during the tidal cycle. Flood and ebb tide over several tidal cycles including one full neap and spring tide was recorded using a high frequency measurement interval of 20 seconds with an averaging interval of 10 seconds. The blanking distance was set to the minimal amount of 0.07 m as the water column was shallow (mean < 0.50 m). The current meters were stably mounted to a mooring with ~25kg weights at the bottom of each mākāhā channel preventing the instruments from moving in the current and ensuring a stable horizontal position within the water column during the deployment period. In order to quantify the physical movement of water passing through the mākāhā channel, instruments were always oriented into the channel. Pictures

illustrating the deployment set-up at each mākāhā are given in Figure 10. We were able to deploy a maximum of three Sontek SW Argonauts at a time. Further instrument specifications and deployment periods are given in Tables 4 and 5.

2.2.5. Rating curves

It is not practical to deploy the Sontek Argonaut SW current meters described in section 2.3 in every mākāhā over extended time periods. These instruments are very expensive and our research team only limited access to them. For long term monitoring, it is more practical to measure water level (m) in the mākāhā with less expensive pressure sensors and relate this to the observed water volume flux ($m^3\ s^{-1}$). This was done by creating rating curves that graphically relate calculated water volume flux for each mākāhā to fluctuating water level in the respective mākāhā for each tidal state (spring flood tide (SF), spring ebb tide (SE), neap flood tide (NF), neap ebb tide (NE)). Rating curves allow for future monitoring of water volume flux through the mākāhā to be accomplished by less expensive pressure sensors alone. Following the methods of Timmerman et al. [19] water volume flux ($m^3\ s^{-1}$) was calculated for each mākāhā, in order to estimate the volume of water moving into and out of each mākāhā channel over a certain time period. Using the Sontek Argonaut SW flux data, water velocity measurements ($m\ s^{-1}$) were multiplied by the area (m^2) of the water column within the mākāhā to obtain water volume flux. The following equation was used:

$$\varphi = wdv \quad \textbf{(1)}$$

where d is the water level vector (m) changing over time with tide, v is the water velocity ($m\ s^{-1}$) through the mākāhā channel and w is the respective mākāhā width (m). Kāne‘ohe Bay is characterized by semidiurnal mixed tides with two high tides and two low tides, of differing heights within a day. As a consequence, the influence of tidal activity from Kāne‘ohe Bay is not consistent between tides and the magnitude of water volume flushing the fishpond fluctuates with different tidal stages. In addition, mākāhā water exchange is characterized by a bidirectional water flow with water flowing into or out of the fishpond during flood and ebb tide. To account for that, water volume flux was calculated for one tidal cycle for the four tidal stages: SF, SE,

NF, NE. When splitting the data set based on their tidal stage, care was taken to always utilize the full tidal amplitude.

In the future, less expensive pressure sensors can be deployed in the mākāhā to measure only water height and water volume flux can be estimated from the rating curves at different tidal stages. For a relatively remote and unprotected field site, the ability to use inexpensive pressure sensors in lieu of more expensive current meters is a distinct advantage. For each mākāhā rating curves were calculated for each of the four tidal stages described previously. Each rating curve was fit using the polyfit function with a best-fit line and 95% confidence intervals in Matlab (MathWorks, Natick, MA). Water volume flow through each mākāhā using these rating curves provides an insight into the relative importance of water volume flux through each mākāhā as well as fishpond volume and residence time.

2.2.6. Mākāhā water volume flux comparison

Establishing a water budget of He‘eia Fishpond requires quantifying the relative importance of water exchange rate at each of the six mākāhā channels. Based on water volume flux (see section 3.1.), mean and maximum flow through each mākāhā were calculated for four tidal cycles (SF, SE, NF, NE). The nature of mixed semidiurnal tides in Kāne‘ohe Bay can cause tidal cycles of varying length. Hence, individual mākāhā flow rates were normalized by calculating the total volume of water (m) moving through the mākāhā channel at a given tidal cycle and the flux per hour rate. Having calculated mean and maximum mākāhā flow rates, the relative importance of each individual mākāhā in overall fishpond circulation was evaluated.

2.2.7. Fishpond volume

Fishpond volumes were calculated based on the method used in Timmerman et al. [19] that used 728 bathymetric depth measurements normalized to mean low low water (MLLW) using data from on a reference HOBO water level logger (Onset, Bourne, MA) deployed at an interior site within the fishpond (Stake 11; N 21.43466, W 157.80699) recording tidal fluctuations during bathymetry mapping. In 2018, we deployed a HOBO water level at the same location to recollect reference water level data over a 10-day period. Reference pressure data was corrected for atmospheric pressure fluctuations using a second HOBO logger situated on land to record

atmospheric pressure fluctuations. In order to calculate the new volumes of He‘eia Fishpond, the difference between pre-restoration (2007) and post-restoration (2018) reference tidal state was applied to the bathymetry data set for the four tidal states (SF, SE, NF, NE). Tidal stages were defined based on criteria described in section 3.1. Tidal data from *Moku o Lo‘e* at HIMB (see section 2.1.) was used as a reference to adjust for differences in tidal amplitude between pre- and post-restoration. Fishpond volumes were calculated using Matlab, adopting a rectangular grid with ~1 m spacing and a natural neighbor interpolation to obtain estimate depths in between measured bathymetry points. A trapezoidal rule was used to calculate fishpond volumes (m^3) for each tidal state. No smoothing was applied, and the small island located in the northwest quadrant of the fishpond was excluded from the volume calculation.

2.2.8. Water exchange and residence time

Methods to calculate the amount of water exchanged and derive the minimum He‘eia Fishpond residence time were adapted from Young (2011) [18]. The amount of water exchanged during ebb flood transition was calculated for neap and spring tide using the following equation:

$$\tau_{HF} = \frac{\text{He‘eia Fishpond Volume Exchanged (spring high tide – spring low tide)}}{\text{He‘eia Fishpond Volume (spring high tide)}} \quad \textbf{(2)}$$

$$_{HF} = \frac{\text{He‘eia Fishpond Volume Exchanged (neap high tide – neap low tide)}}{\text{He‘eia Fishpond Volume (neap high tide)}} \quad \textbf{(3)}$$

From water exchange rates for spring and neap tide we estimated residence time based on the following assumptions: (1) fishpond water column is mixed uniformly, (2) all flood and ebb tides are 6 hours long, (3) mākāhā present the only source of water exchange.
To calculate residence times, the following equation was used:

$$\varphi^x=0.01, \quad \textbf{(4)}$$

where φ is the percentage of water remaining after 1 flushing cycle (12 hours) and x is the residence time in flushing cycles.

2.2.9. Discrete water sampling post-restoration

Characterization of physical and biogeochemical parameters of the fishpond was accomplished through a combination of continuous monitoring via *in situ* instrumentation (see section 2) and discrete water sampling. Water samples were collected for analysis of dissolved nutrients, DNA, and suspended particulates. Sampling was conducted during neap low tide over a period of 3-4 hrs. Neap tides provided minimal water exchange within the fishpond, and therefore present a favorable time window: Sampling during neap tides ensured minimal variability in data on a spatial scale due to small tidal fluctuations and hence provided more reliable data within the fishpond. Sampling sites included 6 perimeter sampling sites at the fishpond mākāhā locations (M01-M06), two end-member sites at He‘eia Stream and Kāne‘ohe Bay (E01, E02), and 10 sites at the pond interior (L01-L10). It was part of our sampling rationale to capture the influence of the mangrove island that is densely populated with a cattle egret *(Bubulcus ibis)* colony. Hence, importance was assigned to sampling with high resolution around the island (L06, L08, L09). We also sampled along a transect from RM 2 to *Kaho‘okele* (former Ocean Break) in order to capture the gradual change in salinity and biomarker distribution from freshwater to seawater (L03, L06, L07, L09, L10). To understand the influence of two distinct water masses (He‘eia Stream freshwater and Kāne‘ohe Bay seawater) on the fishpond, our water sampling plan required measurements of input water end members. End member samples were collected outside the fishpond kuapā. The freshwater end member (E02) was taken upstream from the fishpond, but downstream from the marshland, while the ocean end member (E01) was taken outside *Kaho‘okele* (former Ocean Break), which is representative for Kāne‘ohe Bay surface water. The mākāhā discrete samples (M01-M06) were collected within the mākāhā channel. A map with discrete sampling locations is given in Figure 9 and Table 3. The sampling site was always approached carefully by boat to avoid disturbance of the seabed. Surface water samples were collected by rinsing the hydrochloric acid cleaned polycarbonate collection bottle with ambient surface water three times, then dipping the mouth of the bottle below the water surface and filling the bottle completely. One liter (L) of water was collected at each sample site. Water

samples were stored at 4 °C during sampling. For my comparison of pre- vs. post-restoration, I was able to utilize salinity data and water sampled collected pre-restoration (2014).

2.2.10. Water sample analytical methods

Within 2 hours of collection, all samples were processed and filtered for nutrient analysis and community genetic archive (frozen at -80 °C for subsequent DNA extraction and qPCR analysis). For DNA analysis, 500 mL of the sample was filtered through a 0.45 μm vacuum filter. The vacuum filter was added to pre-labeled tubes and stored in the freezer at -80 °C for later DNA extraction (16S).

2.2.11. Microbial source tracking

For positive control endmembers genomic DNA was extracted (using the DNeasy PowerSoil Kit (QIAGEN, Germantown, MD)) from cattle egret feces that had been collected from the mangrove island in the fishpond interior. Genomic DNA was extracted from two different sampling vials containing cattle egret fecal matter (BF1 and BF2). In the following, extracted DNA was tested with PCR analysis on 9 primers targeting the 16S gene of *Catellicoccus marimammalium, Helicobacter, Bacteroidales and Enterococcus* (Table 6 for a complete list of primers). Both samples (BF1 and BF2) amplified successfully for the GFC primer targeting *Catellicoccus marimammalium* and BF1 sample amplified for the GFD primer targeting unclassified *Helicobacter spp*. [26], Table 7. Furthermore, both samples (BF1 and BF2) amplified for a GenBac3 assay targeting *Bacteroidales* [7,8; Method "B" EPA-822-R-10-003] and an Entero1a assay targeting *Enterococcus* [9,10; Method "A" EPA-821-R-10-004]. As both samples BF1 and BF2 amplified for GFC primer sets, we decided to use the GFC primer targeting the 16S rRNA of *Catellicoccus marimammalium* that had been detected in fecal contamination from gulls in coastal environments for SYBR green qPCR analysis on our water samples. To target broad-spectrum fecal indicator bacteria from other waste sources such as human or other animal waste, water samples were tested with a broad-spectrum GenBac3 assay targeting *Bacteroidales* and Entero1a assay targeting *Enterococcus.*

Genomic DNA from water samples was extracted using the PowerWater DNA Extraction kit (Q, Germantown, MD). Once DNA was ready for downstream application it was stored at -20 °C

until further use. We chose 11 sites for each sampling event: *Kaho'okele* (former OB), *Wai1/*RM2 as well as 9 locations in the fishpond interior. As the sampling grid changed over time, post-restoration (L01-L03, L06-L11, OB, RM2) and pre-restoration (P01-P10, OB) sampling locations differed slightly (Figure 11, Table 3). Sixty-six water samples were prepared for each of the three assays (GFC, GenBac3, Entero1a) using qPCR analysis. The GFC assay was run with SYBR FAST SybrGreen protocol. Fifteen microliter reaction mix containing 10 µL of KAPA SYBRFAST qPCR master mix (2x) universal (KAPA cat no. KK4601), 0.1 µL forward and reverse primer (final concentration of 400 nM), 0.05 µL probe (final concentration of 200 nM), and 4.85 µL water were aliquoted to each well containing 5 µL DNA (diluted 1:5) for a total reaction volume of 20 µL. Cycling parameters were as follows: 95 °C for 3 min for enzyme activation, followed by 40 cycles of 95 °C for 3 sec for denaturation and 60 °C for 20 sec for annealing, extension and data acquisition. For the Entero1a and GenBac3 assay we ran a Taqman protocol (KAPA PROBE FORCE qPCR kit (KAPA cat no. KK4302)) containing 10 µL of KAPA PROBE FORCE qPCR Master Mix (2x) universal, 0.1 µL forward and reverse primer (400 nM), 0.05 µL probe (200 nM), 4.85 µL water, and 5 µL DNA (diluted 1:5). The standard used for GFC primers was acquired from the Green et al. (2012), [26] (accession number JN084062 (uncultured Catellicoccus sp. 16S rRNA gene, partial sequence)).Triplicate standard curves were used to convert threshold cycle (CT) values to copy numbers for each run. Resulting copy numbers were then calculated to concentrations per 100 mL water sample filtered accounting for the proportion of extracted DNA added to each amplification reaction volume. A t-test was done to test statistical significance among mean concentrations before and after the restoration, calculating means and distributions using data from all sites on 3 dates before and 3 dates after for each assay run (GFC, GenBac3, Entero1a). In addition, correlation of GFC/GenBac3/Entero1a distribution with salinity, date and location was tested using a generalized additive mixed model (GAMM) in R (R Foundation for Statistical Computing).

2.3. Influence of restoration regimes on physical and biological parameters in the fishpond (pre- vs. post-restoration)

2.3.1. Comparison of fishpond water exchange, volume and residence time

In order to evaluate how restoration regimes such as removal of mangrove along the He‘eia Stream and the reconstruction of OB have changed fishpond water volume flux, volume and residence time, we compared our data sets taken post-restoration (2018) with data presented in Timmerman et al. [19] taken pre-restoration (2012 and 2007). An overview of meteorological data for all six sampling events pre and post-restoration can be found in Table 8.

2.3.2. Comparison of salinity distribution and abundance of microbial biomarkers

For the comparison of pre- vs. post-restoration, previously collected YSI and discrete water sample data was analyzed. Because of distinctive salinities from two direct sources of water to He‘eia Fishpond (Kāne’ohe Bay and He‘eia Stream), salinity can be used to track the relative proportion of stream versus ocean water within the fishpond. In order to assess if the distribution of stream versus ocean water changed as a result of restoration regimes, we chose three post-restoration sampling events from 2017 (02/18/2017, 04/02/2017, 06/02/2017) and two pre-restoration sampling events from 2014 (08/28/2014, 09/11/2014) with similar meteorological conditions (Table 9). We attempted to select sampling dates that were as similar as possible based on meteorological data described in section 2.1. Rainfall over last 24 hours, cumulative rainfall over last 96 hours, mean Ha‘iku Stream discharge over 24 hours, wind speed and direction, and tide at sampling time were examined when comparing sampling events. In order to contrast baseline and storm conditions, we selected one pre-restoration sampling event in 2014 (10/23/2014) that falls into the category of “storm conditions” that have been defined as a rain event with greater or equal than to 5.1 cm of rainfall over the watershed within a twenty-four hour period [19,24,25]. All other 5 sampling dates can be categorized as baseline or non-storm conditions and have experienced comparable amounts of precipitation. An overview of meteorological data for all six pre- and post-restoration sampling events can be found in Table 9. For analysis of microbial source tracking markers, discrete water samples collected on the same dates were analyzed with microbial source tracking methods.

3. RESULTS

3.1. Characterization of fishpond water volume flux, fishpond volume, residence time and salinity post-restoration

3.1.1. Flow rates and rating curves

Water volume flux (m^3 s^{-1}) relative to the water level (m) for all 6 makāha during each tidal cycle tide can be visualized in the form of rating curves. Site specific rating curves were organized into four tidal stages (SF, SE, NF, NE) and are presented in Figures 12-15. Water volume flux through the mākāhā during flood and ebb tides displayed distinct trends. A positive water volume flux represents flux into the fishpond from Kāneʻohe Bay or Heʻeia Stream. A negative water volume flux represents flux out of the fishpond into Kāneʻohe Bay or Heʻeia Stream.

A characteristic curve shape describes the flow dynamics during flood tidal cycles: At the begin of a flood tidal cycle, water levels are low (~ 0.2 m-0.7 m depending on site) and water levels start rising as water is advected into the fishpond. Water volume flux (m^3 s^{-1}) rapidly increases until approximately the middle of flood tide when reaching a measured water level of ~0.4-0.9 m. After maximum water volume flux velocities are reached (near the middle of flood tide), water volume flux rates decrease until they reach 0 m^3 s^{-1} at slack high tide (~0.5-1.1 m depending on site). At the beginning of an ebb tidal cycle, water volume flux reverses direction and water starts flowing out of the fishpond as water levels drop. Similar to flood tidal cycles, negative water volume flux reaches maximum velocities around the middle of the ebb tide and decreases again before reaching 0 at slack low tide.

Using water volume flux, flow rates per tidal cycle through each mākāhā were quantified for the year of 2018 (post-restoration) and are presented in Table 10. The relative water volume flux for each tidal stage is shown in Figure 16. The highest mean water volume flux during both spring flood and spring ebb, as well as neap flood and neap ebb tidal cycles, was measured at OM1 with +4.18 m^3 s^{-1}, -3.6 m^3 s^{-1}, +2.26 m^3 s^{-1}, and -1.6 m^3 s^{-1} respectively (Table 11). OM1 accounts for roughly half of the total water volume exchanged during one tidal cycle post-restoration with 51%, 44%, 56% and 51% in relative magnitude for spring flood, spring ebb, neap flood and neap

ebb, respectively (Table 11). The newly added mākāhā channel at *Kaho'okele* accounts for the second largest volume of water flux with mean flux velocities of +2.02 $m^3 s^{-1}$, -1.1 $m^3 s^{-1}$, +1.35 $m^3 s^{-1}$, and -0.86 $m^3 s^{-1}$ for spring flood, spring ebb, neap flood and neap ebb tide, respectively. Post-restoration, *Kaho'okele* flux presents roughly a quarter of influx and a third of outflux contributing 28%, 39%, 26% and 33% in relative magnitude for spring flood, spring ebb, neap flood and neap ebb tide, respectively. Triple mākāhā is comprised of three individual mākāhā grouped under the same name. Post-restoration, together they account for the third largest water volume exchanged with mean flow rates of +1.47 $m^3 s^{-1}$, -0.87 $m^3 s^{-1}$, +0.51 $m^3 s^{-1}$, and -0.3 $m^3 s^{-1}$ for spring flood, spring ebb, neap flood and neap ebb tide, respectively and roughly 10% of contribution to total water volume flux (13%, 12%, 10%, 11% for spring flood, spring ebb, neap flood and neap ebb tide, respectively.). Post-restoration, the lowest water volume flux among ocean mākāhā was measured at OM2 with considerably lower mean velocities of +0.39 $m^3 s^{-1}$, -0.17 $m^3 s^{-1}$, +0.05 $m^3 s^{-1}$, and -0.08 $m^3 s^{-1}$ accounting for 4%, 3%, 1%, and 3% volume flux for spring flood, spring ebb, neap flood and neap ebb tide, respectively.

Post-restoration, similar flux rates were measured at RM3 with a relative flux magnitude of 3%, 4%, 7% and 6% and mean flow rates of +0.4 $m^3 s^{-1}$, -0.32 $m^3 s^{-1}$, +0.31 $m^3 s^{-1}$, and -0.17 $m^3 s^{-1}$ for the four tidal stages, respectively. RM2 displayed unidirectional flow into the fishpond only, regardless of tidal state with solely positive velocities of +0.05 $m^3 s^{-1}$, +0.07 $m^3 s^{-1}$, + 0.05 $m^3 s^{-1}$, and +0.88 $m^3 s^{-1}$, accounting for the lowest water volume flux measured (<1%, 1%, 1% and 4% for spring flood, spring ebb, neap flood and neap ebb, respectively). In addition, rating curves for RM2 do not show the typical curve shape described above but have more uniformly distributed velocities without the characteristic peak flux at mid tide.

Post-restoration, the spatial pattern of flushing in He'eia Fishpond is in not uniform across the fishpond but varies greatly according to site: Mākāhā in the northeast quadrant of the fishpond exhibited the highest rates of flushing for all tidal stages with OM1, *Kaho'okele*, and TM together contributing for a water volume flux of 92% of flux at spring flood, 94% at spring ebb, 91% at neap flood and 95% at neap ebb tide. The southern and western edges of the fishpond experience relatively low flushing.

3.1.2. Fishpond volume post-restoration

The large majority of the fishpond area is relatively uniform and shallow bathymetry. Timmerman et al. [19] found that the fishpond was deepest around the mangrove island (~0.90 m) with some other deeper patches in the southern portion of the pond and around Ocean Break which is confirmed by fishpond bathymetry maps calculated for four tidal states (SF, SE, NF, NE) post-restoration (2018) (Figure 17 and 18).

The fishpond is deepest at spring flood tide with an average fishpond depth of 0.89 m ± 0.12 m and minimum and maximum water depths of 0.63 m and 1.46 m, respectively. Consequently, the maximum fishpond volume calculated in section 3.3. is 264,730 m^3 and occurs at spring flood tide. The minimum water retained in the fishpond occurs during the lowest spring low tide (48,060 m^3 -approximately a fifth of the spring flood volume). The average fishpond depth at spring ebb tide is 0.17 m ± 0.12 m and minimum and maximum depths of 0 m and 0.74 m. At neap flood tide the fishpond has a volume of 149,550 m^3, considerably smaller compared to the spring flood tide volume. The average fishpond depth at neap flood tide is 0.50 m ± 0.12 and minimum and maximum depths of 0.25 m and 1.08 m. As expected, neap ebb tide volume is with 63,160 m^3 higher than the spring ebb tide volume. Average fishpond depth at neap ebb tide is 0.22 m ± 0.12 and minimum and maximum depths are 0 m and 0.79 m.

Post-restoration water exchange calculations suggest that approximately 82% of the fishpond water is exchanged during the ebb-flood transition at spring tide. During neap tide ebb-flood transition 58% of the fishpond water is exchanged. Based on water exchange rates, the minimum residence time of He‘eia Fishpond (given the assumptions) amounts approximately 32 hours (1.5 days) and occurs during spring tide when water exchange is maximal. Following the methods used by Young (2011) [18], we defined the time for one flushing cycle as 12 hours: The time that it takes to flush out 82% of fishpond water during spring ebb tide and to replenish that water again with new Kāne‘ohe Bay water during spring flood tide. Based on the assumption that the incoming water would be uniformly mixed with the 18% of water that had remained in the fishpond during the first flushing cycle, approximately three flushing cycles are required to mix the initial 18% of water to a <1% dilution. Therefore, the minimum residence at He‘eia Fishpond is equal to under three flushing cycles and approximates 32 hours.

In contrast, it takes over 5 flushing cycles (2.5 days, 64 hours), to mix the 42% of water retained during a neap flushing cycle down to 1% dilution. Therefore, residence time at He‘eia Fishpond is with approximately 2.5 days maximal at neap tides when water exchange is minimal. Volumes and water exchange rates can be found in Table 12 and 13.

3.1.3. Salinity distribution post-restoration

Water mixing within He‘eia Fishpond is best represented in salinity: Surface salinity distribution during three sampling events post-restoration (2017) displayed a strong spatial gradient (Figure 19). Salinities in the surface layer (top 25 cm) of the fishpond range from 0.10–32.59 ppt, with an overall average of 20.50 ppt ± 10.41 ppt. Highest measured surface salinities occur along the ocean side of the fishpond near OB, and OM1 (sites M05, L10, Figure 9). In contrast, the lowest measured surface salinities occur on the river site of the fishpond near RM2 (site L07, Figure 9). The freshwater wedge from the river extends past the mangrove island, where salinities rise to 15–20 ppt (sites L06, L08, L09). Further east salinities are rising to above 20 ppt (sites L01 and L05) and 25–30 ppt (sites L02, L03, L04, L11, M03, Figure 9), Figure 19. The strong spatial gradient suggests that ocean water from Kane’ohe Bay dominates the southeastern side of the fishpond, whereas freshwater from He’eia Stream is more prevalent along the northwestern side of the fishpond with areas of mixed salinities, where these two distinct water masses come together.

In contrast, the bottom waters have higher average salinities of 25.17 ppt ± 8.12. Bottom salinities are more homogenously mixed displaying little spatial variability compared to surface salinities. The majority of the fishpond interior has salinities of 25-20 ppt (Figure 19). While bottom waters have distinctly higher salinities, as one would expect, the influence of freshwater from He’eia stream and ocean water from Kaneohe Bay is still somewhat visible: The highest measured bottom salinities occur along the ocean side of the fishpond near OB, OM1 and the lowest measured bottom salinities occurs at the river influenced site of the fishpond at RM2. There is little temporal variability visible in bottom salinities. All three sampling events display a similar spatial salinity distribution (Figure 19).

A t-test for surface salinities indicated no significant variation in mean surface salinities across all sampling locations among the three post-restoration sampling events (2017) (pairwise p-values > 0.78, see Table 9 for an overview of sampling dates and meteorological conditions). Surface salinities for all three sampling events (event 1-3) were significantly different from bottom salinities for all three sampling events (event 1-3), pairwise p-value = 0.007. Analysis of meteorological conditions, shows minor variability in daily rainfall and stream discharge. Daily rainfall is below 0.1 cm for all three sampling events (0.46 cm, 0 cm and 0.91 cm for event 1-3) and Ha'iku stream discharge ranges from 0.07 to 0.06 $m^3 s^{-1}$ (event 1 and 2). Stream discharge data for event 3 was not available. All three events can be categorized as non-storm or baseline condition with less than 5.1 cm of rainfall over 24 hours [18,19]. Wind direction varied between northeast (NE) and east (E) with 3-6 knots (Table 8).

3.2. Influence of restoration regimes on physical and biological parameters in the fishpond (pre- vs. post-restoration)

When comparing site specific volume flux rates pre-restoration (2012) to post-restoration (2018), it becomes evident that the relative magnitude of water volume flux specific to each mākāhā changed due to restoration practices: The total amount of water volume exchanged in a complete tidal cycle decreased from 241,413 m^3 pre-restoration to 194,700 m^3 post-restoration for flood tide and decreased from -241,685 m^3 pre-restoration to -173,080 m^3 post-restoration (Table 10 and 14). Pre-restoration, OB was the "mākāhā" facilitating the largest amount of volume exchange contributing approximately ~80% to total water exchange at both flood and ebb tidal cycles (81.94% for flood, 79.76% for ebb) with mean water velocities of 11.53 $m^3 s^{-1}$ and -13.55 $m^3 s^{-1}$, Table 15. Pre-restoration OM1 contributed the second largest amount of volume exchange with 12.88% for flood and 11.12% for ebb tide and mean velocities of 1.75 $m^3 s^{-1}$ and -0.5 $m^3 s^{-1}$ (Table 15). While contributing only 10% to water exchange pre-restoration, post-restoration OM1 is presently the site with largest water volume exchange. Post-restoration, OM1 facilitated about half of the volume flux (50.24% at flood, 44.1% at ebb tide) with much higher mean velocities of 4.18 $m^3 s^{-1}$ and -3.6 $m^3 s^{-1}$ (Table 10 and 14) than pre-restoration. In contrast to pre-restoration numbers, OB (now *Kaho'okele*) accounts now for the second largest volume exchanged (27.93% and 39.01% for flood and ebb tide respectively) with lower mean velocities

of 2.02 m^3 s^{-1} and -1.1 m^3 s^{-1} compared to pre-restoration. The relative contribution in magnitude of three channels constituting triple mākāhā increased about six-fold for flood tide and 5-fold for ebb tide from pre-restoration to post-restoration (from 1.71% to 12.54% for flood tide and 2.41% to 11.68% for ebb tide, Table 15). OM2 did not experience significant changes due to restoration: While accounting for 1.69% at flood and 2.03% for ebb pre-restoration, it now accounts for 3.61% and 2.76% at flood and ebb, respectively (Table 15). Mean flux velocities ranged from -0.12 m^3 s^{-1} to 0.28 m^3 s^{-1} pre-restoration and are now -0.17 m^3 s^{-1} to 0.39 m^3 s^{-1}.

Water volume flux at the two river mākāhā at RM3 overall has increased from pre-restoration to post-restoration: Water passing through RM3 increased from 0.93% pre-restoration to 5.1% post-restoration for flood tide, and 2.4% pre-restoration to 5.7% post-restoration for ebb tide. Velocities increased from 0.09 m^3 s^{-1} and 0.1 m^3 s^{-1} pre-restoration to 0.4 m^3 s^{-1} and 0.32 m^3 s^{-1} post-restoration. Pre-restoration RM2 accounted for 0.85% of flux during flood tide and accounts for a slightly decreased flux of 0.67% post-restoration for flood tide. For ebb tide, the flux reversed from 2.28% pre-restoration to -3.25% post-restoration. It is notable that, while water was draining out of the fishpond at RM2 during ebb tide in pre-restoration, post restoration measurements revealed only positive flux velocities at RM2, suggesting a solely unidirectional flow into the fishpond independent of tidal state post-restoration.

Looking at the overall volume, river mākāhā only played a minor role in water exchange for both pre- and post-restoration. The largest shift in water exchange occurred at the ocean mākāhā: Ocean Break, which pre-restoration exchanged the most water during spring tide (~80%), before it was repaired. Post-restoration, OM1 now exchanges the greatest water volume (~50%) and *Kaho'okele* the second largest (~30%) amount of water exchange. Post-restoration OM1 and *Kaho'okele* together accounting for the large majority of water exchange (~80%). The full set of rating curves for spring flood and ebb tide pre-restoration is presented in Figures 20-21.

Meteorological conditions during water volume flux sampling events show some variability over time (see Table 8). While daily rainfall ranged from 0.05 cm to 1.32 cm in 2012 (pre-restoration) (mean 0.76 ±0.6), it ranged slightly higher from 0 cm-2.29 cm (mean 1.23±0.87) in 2018 (post-restoration). Similarly, Ha'iku Stream discharge ranged from 0.04 m^3 s^{-1}- 0.07 m^3 s^{-1} (mean 0.06

±0.013) in 2012 (pre-restoration), and from 0.06 m^3 s^{-1}-0.11 m^3 s^{-1} (mean 0.085± 0.03) in 2018 (post-restoration). Wind direction ranged from E to NE (average wind direction ~50°) with magnitude ranging from 10 to 13 knots pre-restoration and from E to NE (average wind direction ~60°) with magnitudes of 3-13 knots post-restoration.

Restoration regimes resulted in a considerable change of fishpond volume from pre-restoration (2007) to post-restoration (2018): Spring ebb tide fishpond volume decreased from is 64,070 m^3 pre-restoration to 48,060 m^3 post-restoration. Spring flood tide volume decreased from 282,720 m^3 pre-restoration to 264,730 m^3 post-restoration. Fishpond volumes decreased from 78,050 m^3 pre-restoration to 63,160 m^3 post-restoration at neap ebb tide and increased at neap flood tide from 133,890 m^3 to 149,550 m^3 (Table 12).

Water exchange rates during ebb flood transition experienced a 4.51% increase (from 77.34% pre-restoration to 81.85% post-restoration, Table 13) at spring tide. During neap tide water exchange increased 16.06% (from 41.71% pre-restoration to 57.77% post-restoration, Table 12). As a result, minimum water residence time decreased from 38 hours at spring tide pre-restoration to 32 hours (~1.5 days) at spring tide post-restoration and maximal residence time during neap tides decreased from 102 hours (~8.5 days) at spring tide pre-restoration to 64 hours (~5.5 days) at spring tide post-restoration.

Surface salinity distribution during three sampling events pre-restoration (2014) displayed the same spatial pattern as described for post-restoration (2017) in section 1.3. Similar to post-restoration, highest measured surface salinities pre-restoration occur along the ocean side of the fishpond near OB, and OM1 (site P10). In contrast, the lowest measured surface salinities occur on the river site of the fishpond near RM2 (site P3), Figure 22. However, overall less freshwater influence and therefore a weaker gradient is evident pre-restoration (Figure 19 and 22). Non-storm event salinities (event 4 and 5) for the surface layer (top 25 cm) had an average of 27.4 ppt ± 4.86 pre-restoration, higher than the average salinity measured post-restoration sampling events (20.5 ppt ± 10.41 ppt). Before and after restoration, the freshwater wedge from the river extends only to the western edge of the mangrove island, where salinities rise quickly to 20–25 ppt (sites P2, P4, P5). Further east salinities are rising to 25–30 ppt (sites P1, P6, P7, P8, P9)

(Figure 19 and 22). While the bottom layer displays some spatial gradient post-restoration (Figure 19), pre-restoration bottom salinity distribution is entirely homogeneously mixed with no freshwater influence visible for all three sampling events pre-restoration (Figure 22). Average salinities are higher with 31.99 ppt ± 1.82 higher pre-restoration than post-restoration (25.17 ppt ± 8.12 ppt). A t-test comparing surface non-storm pre-restoration (event 4 and 5) to surface non-storm post-restoration (event 1-3) shows that they significantly differ (pairwise p-value < 0.01). Bottom non-storm pre-restoration (event 4 and 5) and bottom non-storm post-restoration (event 1-3) sampling events show statistically significant variation (pairwise p-value <0.1) as well. The storm event (event 6) pre-restoration has an average salinity of 23.45 ppt ± 6.9 ppt for the surface and 31.61 ppt ± 1.2 ppt for the bottom, which is lower than for the non-storm events but yet higher than the post-restoration surface salinity average. A t-test indicates that the storm-event has no significantly different salinities than the non-storm events at the surface (pairwise p-value = 0.1298) or the bottom (pairwise p-value = 0.497). When comparing meteorological conditions pre- and post-restoration, non-storm events display minor variability (Table 9): Daily rainfall is 0-0.61 cm (compared to 0-0.91 in 2017) and Ha‘iku stream discharge is 0.05-0.06 m^3 s^{-1} (compared to 0.6-0.7 in 2017). Solely one event in 2014 (event 6) has considerably higher rainfall with 42.3 cm per 24 hours and can therefore be categorized as storm event [18,19].

Temporal analysis of GFC bacterial biomarker concentrations shows strong variability between sampling events. Sampling events 1 and 2 (pre-restoration: 08/28/2014 and 09/11/2014, Table 9) have the highest mean concentration of 207141±236444 copies 100 ml^{-1} and 369509±141863 copies 100 ml^{-1} respectively (Figure 23). Sample event 3-6 (10/23/2014, 02/17/2017, 04/02/2017, 06/02/2017, Table 9) have lower mean concentrations of 38182±23836 copies 100 ml^{-1}, 16895±16216 copies 100 ml^{-1}, 40138±43582 copies 100 ml^{-1}, 37244±48923 copies 100 ml^{-1} respectively. Welch t-test reveals that sampling event 1-3 (pre-restoration) are significantly higher than sampling event 4-6 (post-restoration), pairwise p-value<0.01. Furthermore, the Welch t-test indicates no significant difference between the pre-restoration storm event (event 3) and all non-storm events (event 1-2, 4-6; Table 9), pairwise p-value>0.05. GFC concentration distribution displays a distinct spatial gradient with lower Log GFC copies 100 ml^{-1} at the saltwater dominated site of the fishpond, mixed concentrations in the pond center and higher concentrations at the freshwater dominated site of the pond (events 1, 4, 5, 6; Figure 24). In

addition, sampling event 5 and 6 have a distinct feature: A circular shaped area of lower concentrations at the pond interior that sets itself apart from surrounding higher concentrations (Figure 24). Sampling event 2 and 3 display a uniform Log GFC copies 100 ml^{-1} with no spatial gradient visible (Figure 24).

The highest GenBac3 concentrations were measured for sampling events 4 and 5 (400933±698362 copies 100 ml^{-1} and 419343±588595 copies 100 ml^{-1}). Sampling events 3 and 6 had intermediate GenBac3 concentrations (284881±342373 copies 100 ml^{-1} and 293283±369297 copies 100 ml^{-1}) and sampling event 1 and 2 had overall lowest GenBac3 concentrations (70718±82029 copies 100 ml^{-1}, 121034±158329 copies 100 ml^{-1}), Figure 25. Welch t-test indicates no significant difference between sampling events 1-3 (pre-restoration) and sampling events 4-6 (post-restoration), pairwise p-value>0.05. However, the Welch t-test indicates that the storm event (event 3) does differ significantly from the non-storm events, pairwise p-value<0.01. All 6 sampling events show a spatial gradient to varying degrees with higher concentrations (Log GenBac3 copies 100 ml^{-1}) at the freshwater site of the fishpond and lower concentrations on the saltwater influenced site of the pond (Figure 26). Sample event 1 and 6 have the more pronounced spatial gradients than sampling events 2-5. In line with what has been observed for the GFC distribution, sample event 5 and 6 have a distinct circular feature of lower concentrations in the pond interior (Figure 26). Some change in spatial distribution is visible, but average abundance of *Bacteroidales* did not change from pre- to post-restoration.

Entero1a bacterial biomarker concentrations were 8115±8377, 21165±38107, 11604±7123, 10111±8266, 25924±28395, and 46257±69351 copies 100 ml^{-1} for sample event 1-6 respectively. Welch t-test indicated no significant difference between sampling event 1-3 (pre-restoration) and sampling event 4-6 (post-restoration), pairwise p-value> 0.05. However, the storm event (event 3) does significantly differ from non-storm events, pairwise p-value<0.01, Figure 27. As observed for GFC and GenBac3, Entero1a shows a characteristic spatial gradient with higher concentrations on the North-Western site of the fishpond that is largely fresh water influenced and lower concentrations in the South-Eastern site of the fishpond that is saltwater influenced (Figure 28). Sample event 1 and 6 have the more pronounced spatial gradients than sampling events 2-5. In line with what has been observed for the GFC and GenBac3 distribution,

sample event 5 and 6 show a distinct circular feature of lower concentrations in the pond interior (Figure 28). Some change in spatial distribution is visible, but average abundance of *Enterococcus* did not change from pre to post-restoration.

4. DISCUSSION

4.1. Characterization of fishpond water volume flux, volume, residence time and salinity post-restoration

4.1.1. Rating curves and mākāhā flux rate comparison

One of the primary goals of this study was to quantify the water volume flux ($m^3 s^{-1}$) moving into and out of each mākāhā, over extended time periods. The construction of rating curves provided a practical solution in order to be able to do future monitoring of water volume flux at He‘eia Fishpond derived from water level alone (see section 2.2.). Discharge measurements over a range of water level have been proven to be essential as a basis for construction of accurate rating curve [31]. Kāne‘ohe Bay is characterized by mixed semidiurnal tides [32] meaning there are two flood tides and two ebb tides, of differing heights, within a day. Hence, the influence of tidal activity from Kāne‘ohe Bay on He‘eia Fishpond is not consistent between tides causing the magnitude of the flow rate to vary over tidal amplitude. As water volume flux fluctuated with already small changes in tidal amplitude, we decided to create two sets of rating curves for each mākāhā: Spring ebb and flood rating curves and neap ebb and flood rating curves. We did not develop specific rating curves for water volume flux at intermediate (between spring and ebb) tides. Hence, prediction needs to be based on the rating curves developed for neap and spring tide, with water volume flux likely falling somewhere into the intermediate spectrum when tides are intermediate. Nevertheless, this comprehensive set of rating curves (site specific for flood and ebb at spring and neap tides) allows us to make predictions about water volume flux passing through each mākāhā by monitoring water level through an inexpensive set of pressure sensors alone. Spring and neap tides are characterized by similar trends, with spring tides having a larger range of tidal amplitude and water volume flux rates. For simplicity, we base our discussion hereafter on values from spring tides. However, the same reasoning can also be applied to neap tidal cycles keeping in mind that tidal amplitudes and hence water volume flux are smaller at neap tide.

Post-restoration rating curves show a clearly tidally driven water volume flux signal with highest water volume flux at the middle of ebb and flood tides for OM1, OM2, *Kaho‘okele* and TM and

RM3 (Figures 12-15). Due to the nature of the tidal wave, water velocities are greatest around mid-tide and decrease towards slack tides. For that reason, we observe the greatest water volume flux rates at "mid tide" creating a characteristic "C" shape to the rating curves (Figures 12-15). Standard deviations are smaller at low or high tide compared to mid tide, suggesting that there is less variability in the water volume flux during the slack high and slack low tides. Our findings of a tidally driven system during baseline conditions are consistent with previous circulation studies conducted at He'eia that have quantified flux at mākāhā in a similar manner [18,19]. Moreover a study by Ertekin et al. (1999) [33] identified tidal forcing as the primary driver for fishpond circulation at Ocean mākāhā and runoff location and stream velocity as important drivers of flux for river bordering mākāha. Our flux measurements were all conducted at non-storm/baseline conditions (Table 8), making any conclusions about relative influence of stream discharge on fishpond circulation during storm events difficult. However, a previous study found that the relative importance of physical forcing changed during storm events, when water flushing was solely driven by stream discharge rates during a storm for up to 24 hours before tidal forces became dominant again [18]. Another quantitative study measuring flux during a storm event would be necessary to quantify how the relative flux of river mākāhā alters fishpond circulation with strong river flushing present.

Flux rates during spring flood and spring ebb tides from mākāhā bordering Kāne'ohe Bay (OM1, OM2, OB, TM, Table 11, Figure 16), suggest that the fishpond is more influenced by oceanic inputs (>95% of total mean flux) than freshwater inputs (<5% of total mean flux) from He'eia Stream (Table 11) at non-storm/baseline conditions at both pre and post-restoration. Mākāhā water volume flux comparison post-restoration (Figure 16) identified OM1 as primary driver of water exchange (contributing to ~50% of total flux). *Kaho'okele* accounted for the second largest water volume exchanged (~30%), making the north-eastern portion of the fishpond the primary area of flushing (together ~80%). A combination of factors may be at play here: Both mākāhā have large cross-sectional areas (width OM: 6.48 m; width *Kaho'okele*: 3.05 m, Table 1) allowing them to flush a greater water volume at any given time than smaller mākāhā. In addition, OM1 has a bearing of 63° (Table 1), thus facing NE, closest to the predominant trade wind direction (60°) during measurement periods (Table 8). Wind blowing from the NE across Kāne'ohe Bay, can accelerate (or dampen) water flow through OM1, which is aligned with the

predominant wind direction of 60°. This hypothesis is supported by Yang (2000) [34], who suggested that the rate of water flow through the mākāhā may be altered by wind accelerating or dampening flow when the body of water was large enough. Both Kāneʻohe Bay and Heʻeia Fishpond (88 acres) are large enough, and shallow enough, to be affected by wind stress in such a way, which may be a secondary driver after the tidally driven flux patterns observed. *Kahoʻokele* has the only channel floor that is deeper than the adjacent sediments to both sides (fishpond interior and Kāneʻohe Bay), the mākāhā floor thus provides no resistance to water volume flux and could enhance flux through *Kahoʻokele.*

In contrast, TM and OM2 have considerably smaller relative flux (together accounting for ~ 15%, Table 10). TM combined accounts for ~10% of flux (Table 11) with each individual channel accounting for only 3-4% of water volume flux exchanged. Among all ocean mākāhā, OM2 accounts for the smallest relative flux (~3%, Table 11) as it has the smallest cross-sectional area (2 m, Table 1). During our measurement period (non-storm conditions, Table 8) river mākāhā have the smallest relative flux rate (RM2 and RM3 together ~5%). Flux through RM3, the most seaward mākāhā along the Heʻeia Stream, is affected by tidal activity due to its proximity to Kāneʻohe Bay, making it the only freshwater mākāhā that allows bi-directional water flow. At non-storm conditions, the relative flux of water passing through RM3 during flood tide is balanced by the amount of water flowing back out during ebb tide (Table 11). However, at flood tides the water must overcome water flowing out of Heʻeia Stream in order to enter the fishpond, while Heʻeia Stream aids downstream flow out of the mākāhā during ebb tides. Although beyond the scope of this study, the relative contribution of river mākāhā vs. ocean mākāhā as well as the balance between ebb vs. flood exchange is likely to change, if Heʻeia stream discharge increases during storm events. In contrast to all other mākāhā, RM2 presented a distinct pattern, with little-to-no tidal signal visible and solely unidirectional flow into the fishpond (Figures 12-15). Located furthest upstream and being built with a dam like structure elevated from the fishpond (Figure 5), RM2 can only exhibit unidirectional flow from Heʻeia stream into the fishpond. As a consequence, the amount of flux passing through RM2 will largely depend on the amount of precipitation in Heʻeia ahupuaʻa and Heʻeia Stream discharge [19,33,34].

Although site specific water volume flux into the fishpond during flood tide is largely balanced by flux out of the fishpond during ebb tide post-restoration (Table 10 and 11), some mākāhā display a larger/smaller relative outflux compared to influx. This imbalance is most evident for *Kaho'okele*, which accounts for 28% of influx, and 39% of outflux during spring tide. In contrast, OM1 accounts for 40% of influx and 44% of outflux during spring tide. This pattern, present for both spring and neap tidal cycles can be explained by tradewinds accelerating flow into the fishpond at OM1 during flood tide, which is, as previously discussed is aligned with the prevailing wind direction during sampling (63°, Table 1). However, during ebb tide the wind force is dampening outflow at OM1, and a small proportion of water flux is redistributed to other mākāhā channels thereby compensating for the reduced outflow at OM1 (Table 11, Figure 16).

Assuming the He'eia Fishpond water balance is in steady state, the influx rates should be equal to outflux rates. However, when He'eia Fishpond spring and neap tidal cycle flow calculated as the sum of flow (m^3) over all mākāhā are compared to one another, a difference of negative 16,760 m^3 (~8% of total flow) between spring flood and spring ebb tide and positive 18,554 m^3 (~13% of total flow) for neap tide becomes evident. A number of factors can explain the discrepancy: Most importantly, the mixed semidiurnal nature affecting He'eia Fishpond, causes great variation in tidal length (Table 10), giving rise to some uncertainty in the final water volume flux rates calculated. In addition, gains or losses of water through holes in the kuapā are possible. Another factor not accounted for is the influence of submarine groundwater discharge (SGD) into He'eia Fishpond. A previous study quantifying SGD at He'eia Fishpond using radon isotope measurements found that the amount of water flux from SGD was equal to that of He'eia Stream discharge [23]. In addition, the flow at RM1, that could not be quantified due to its diffusive nature, has not been accounted for in our water budget. Hence, both SGD and diffusive flow at RM1 cause uncertainty in flow rate calculations and could likely contribute to the imbalance in water budget. Although every effort was made to choose tidal cycles similar in length and amplitude for rating curves, instrument limitations did not allow us to measure all mākāhā simultaneously. Therefore, rating curves were calculated using time series data from different time periods (Table 8) leading to some degree of variability in tidal length and amplitude among sites.

4.1.2. Fishpond volumes, exchange and residence time

Estimations of residence time were based on 3 main assumptions: (1) fishpond water column is mixed uniformly, (2) all flood and ebb tides are 6 hours long, (3) mākāhā present the only source of water exchange. However, from salinity measurements at surface vs. bottom it is evident that the water column is mildly stratified and not homogeneously mixed. Furthermore, upon analyzing the variability in length of tidal cycles, it becomes clear that there is a large range in variability (from 4.43-17.46 hrs. for tidal cycle length, Table 10). Lastly, it is likely that there are other indirect sources of water exchange as SGD and RM1. As introduced through freshwater runoff, in stratified waters fecal indicator bacteria (FIB) are likely to accumulate in the fresh the water lens at the surface of the fishpond raising a need to differentiate between surface vs. bottom water residence time. Although this distinction is beyond the scope of this study, these qualitative calculations allow us to estimate minimum (based on spring tide with maximal exchange) and maximum (based on neap tide with minimal exchange) residence time of He‘eia Fishpond waters. As residence times have been estimated in a previous study using the same method, they allow us to evaluate how restoration regimes have impacted fishpond overall residence time.

4.1.3. Salinity distribution

He‘eia Fishpond has a estuarine like environment, characterized by two water masses that mix: Freshwater from He‘eia Stream enters at the northwestern portion of the fishpond, while the eastern site of the fishpond is dominated by saltwater from Kāne‘ohe Bay [19]. These two water masses of distinct salinities mix. The resulting horizontal gradient has a wide range of salinities in the fishpond (Figure 19). The distinct density of the two water masses also causes a vertical gradient or stratification [38]. Hence, water mixing within He‘eia Fishpond can be best represented by horizontal and vertical salinity gradients allowing us to assess the relative importance of freshwater vs. saltwater.

4.2. Influence of restoration regimes on water volume flux, fishpond volume and residence time: A comparison between pre- and post-restoration

For the water volume flux rate comparison, efforts were made to choose tidal cycles similar in tidal amplitude for the construction of rating curves pre and post-restoration (Table 15). However, tides -even if both selected from the same tidal category (spring and neap)-can have variable amplitudes leading to a degree of uncertainty with rating curve comparison. Nevertheless, our results present a good indication of changing circulation dynamics as a result of large scale restoration regimes.

Comparison of rating curves indicates that the repair of Ocean Break and the integration of *Kaho'okele* affected the relative flux distribution of the mākāhā (Table 15). As the repaired wall section at Ocean Break used to be lower than the remaining fishpond kuapā, the entire 56 m wide section of Ocean Break essentially functioned like a mākahā, when tides in Kāne'ohe Bay were high enough to flood the provisional elbow wall at Ocean Break. The large volume of water caused the enormous water volume flux at spring tides observed pre-restoration (~80% from OB alone, Table 15). In 2015, this expansive section of the wall was repaired and *Kaho'okele* was built, shifting relative mākāhā exchange rates at *Kaho'okele* to ~30% post-restoration. This dynamic is also reflected in mean water volume flux rates: Pre-restoration, OB had the highest mean water volume flux rates of ~12-14 m^3 s^{-1} (Table 14), while the *Kaho'okele* flux rates post-restoration are dramatically lower (now ~ 1 m^3 s^{-1}, Table 10). Mean water volume flux rates at other mākāhā generally increased from pre-restoration to post-restoration, an indication that nearby mākāhā are compensating for some of the flux that decreased so drastically at OB. However, the general "C" shape of rating curves remained similar, revealing that the system is largely tidally driven both for pre-restoration and post-restoration at non-storm/baseline conditions [19,34,39].

Ocean Break repair also affected fishpond volumes considerably (Table 12): The addition of another *Kaho'okele*, causes more and faster outflux during both neap and spring low tide leading a lower volumes post-restoration. Similarly *Kaho'okele* allows more influx during neap high tide compared to before, resulting in a larger fishpond volume post-restoration (Table 12). Only during spring high tide pre-restoration, when water level was high enough to crest over the 56 m Ocean Break in 2012, which allowed massive volumes of water (~12-13 m^3 s^{-1}) to crest over the wall. These water masses cannot be compensated entirely with flow (1-2 m^3 s^{-1}) through the

much smaller *Kaho'okele* (3.05 m) channel causing an overall larger fishpond volume post-restoration (2018) (Table 12). This dynamic is also reflected in fishpond exchange rates and residence times: While total exchange rates increased 5% during spring tides moving from pre to post-restoration, they increased 16% during neap tides. Minimum residence times during spring tides decreased from 38 hours pre-restoration to 32 hours post-restoration, a difference of 6 hours. Maximum residence times during neap tides decreased from 102 hours (~4.2 days) pre-restoration to 64 hours (~2.6 days) post-restoration, a difference of 38 hours (~1.6 days). It is therefore important, to differentiate between tidal states when looking at the effects of restoration on the physical environment of the fishpond: The difference in change for neap tide is much greater because the effect of *Kaho'okele* as a new mākāhā channel, is fully noticeable. At spring tides during pre-restoration, the water was cresting over the wall at Ocean Break, hence the increase of relative flux through the new mākāhā channel less profound when comparing spring tide exchange between pre and post-restoration. Before Ocean Break repair, the fishpond acted largely as an unconfined system during spring tides, when the spring flood tide exceeded the height of Ocean Break. During neap tides in however, the fishpond was more confined with less exchange and circulation in the south eastern portion of the fishpond. The repair of the wall section and the integration of *Kaho'okele* changed these dynamics: The fishpond in its current state presents a confined system at all tidal states with adequate water exchange in the south eastern region due to the addition of *Kaho'okele*. Our findings are supported by a circulation study that modeled circulation patterns at two different Ali'i fishponds in Molokai and concluded that the number of mākāhā plays a significant role in improving tidal circulation [39]. Furthermore, mākāhā distance and location in relation to the physical forces at work (tidal activity, wind, fishpond bathymetry, stream location), was found to effect circulation inside the fishpond [39].

In comparison to the ocean mākāhā, the river mākāhā play a minor role in water exchange in both pre-restoration and post-restoration during baseline/non-storm conditions. This can be attributed to the fact, that for our study, flux measurements were taken during non-storm/baseline conditions with rainfall smaller than 5.1 cm within 24 hours [19]. As discussed before, the relative importance of river flushing on fishpond circulation is likely to change drastically during a storm event [19]. The volume flowing through RM3 increased from pre-restoration (~1-2%) to

post-restoration (~5%), Table 15. This trend could be attributed to the progressive removal of mangroves around the river mouth especially, where RM3 is located (Figure 1). Through their dense root system and high sediment accumulation rates, mangroves in Hawai‘i are known to inhibit water circulation [15,40], hence likely inhibiting water volume flux at river mākāhā before mangrove clearance in that region. Flux was measured during non-storm conditions in both pre-restoration and post-restoration (Table 8), however minor variability in precipitation and stream discharge between the sampling dates is inevitable. It is therefore possible, that minor increases in precipitation (Table 8) may have contributed to increased flux rates in 2018. Hence, it is difficult to completely isolate the effects of mangrove removal on river mākāhā discharge. However, RM2, which has not been cleared from mangroves yet, shows little change in discharge between pre and post-restoration, suggesting that mangrove removal at RM3 is at least partially responsible for the increased flux rate observed at RM3 stressing the positive impact mangrove removal can have with regards to increasing water flow. Increased freshwater flux is also reflected in the salinity distribution, which shows a much stronger freshwater signal around river mākāhā in post-restoration compared to pre-restoration (Figure 19 and 22) despite comparable weather conditions among sampling events (Table 9). Every effort was made to compare sampling dates for salinity and discrete water samples that were as similar in daily precipitation and Ha‘iku Stream discharge as possible. As He’eia Fishpond had previously been observed to recover to baseline conditions ca. 4 days after a storm event [19], cumulative rainfall over 4 days preceding sampling was taken into consideration in addition to daily rainfall and stream discharge. While some extent of variability in weather is inevitable, we believe that the non-storm event sampling dates chosen are comparable, hence the change in salinity significant. Microbial source tracking (MST) is a method used to identify fecal pollution sources in environmental waters to assess water quality and associated human health risk [41]. MST often utilizes indicator microorganisms, which are nonpathogenic, easily to quantify and have decay rates similar to those of the pathogens of interest. Hence, they can be strongly associated with the presence of pathogenic microorganisms and are used in microbial source tracking to quantify pathogenic microbes [42]. Paepae O He‘eia has the long-term goal of producing fish for sale and need to comply with food safety standards. In addition, the fishpond hosts numerous educational activities and needs to be safe for the public. Hence, an assessment of water quality at the fishpond is of particular importance.

Microbial analysis dates were identical to sampling events used for salinity analysis. The rational was two-fold: First, sampling dates chosen were all non-storm/baseline conditions (except one storm event during hurricane 'Ana' pre-restoration on 10/23/2014) that had experienced similar amounts of rainfall and stream discharge and were most comparable (Table 9). Secondly, it allowed us to correlate salinity and microbial concentrations, which was of importance as the survival of indicator microorganisms in aquatic systems has been shown to be influenced by both biotic and abiotic factors [44–46]. We expected higher concentrations of bacterial biomarkers during storms due to increased river water run-off into the fishpond [47,48]. This allowed us to contrast distributions of bio-indicator bacteria across the pond during baseline conditions with little to no rain and storm conditions with heavy rainfalls. Our ultimate goal was to compare spatial distribution of fecal indicator bacteria (FIB) before and after restoration regimes in order to determine a linkage between changing water volume flux, fishpond volume, residence time and water quality as a result of restoration.

Two broad spectrum markers targeting *Bacteroidales* (GenBac3) and *Enterococcus* (Entero1a) were used in this study as an indicator of fecal pollution. *Enterococcus* are Gram-positive bacteria common in the feces of warm-blooded animals, that have been widely used for water quality testing and targeted by the Environmental Protection Agency (EPA) for regulatory action [44,49]. As the fishpond is home to a large cattle egret colony, a potential source of microbial contamination, we wanted to optimize a bacterial biomarker that was specific to cattle egrets (*Bubulcus ibis*) and could be used to assess the impact of the cattle egret colony on the fishpond's water quality. While we were not able to find primers specific to cattle egrets, we composed a list of primers targeting the 16S rRNA gene of *Catellicoccus marimammalium* (GFC), an uncharacterized Gram-positive facultative anaerobe in the order of *Lactobacillales (Fusobacterium)* [50] originally developed to detect fecal contamination from gulls in coastal environments [26,51–55]. Our results revealed no significant change in average abundance for *Bacteroidales* and *Enterococcus* and a significant decrease for *Fusobacteria* in number of copies/100ml pre- vs. post-restoration (Figure 23, 25, 27). While these results are ambiguous and not sufficient to draw firm conclusions about the influence of restoration regimes on water

quality, there are multiple processes that could be potentially important in determining the distribution of microbial biomarker quantities across the fishpond observed:
Overall salinity decreased significantly from pre- to post-restoration. That trend might contribute in explaining the overall increase in *Bacteroidales* and *Enterococcus*, as these microbes are most likely introduced to the fishpond environment via terrigenous freshwater run-off. In addition, fresh water conditions are generally more favorable for these microbes to survive [46]. This tendency is also reflected in the spatial distribution, as numbers are generally higher on the freshwater dominated site of the pond and lower on the saltwater dominated site for all three biomarkers (Figures 24, 26, 28). At the same time, the increase of water exchange and decrease in residence time from pre- to post-restoration leads to an overall decrease in microbial biomarker concentrations. The *Fusobacterium* specific to birds decreased significantly from pre- to post-restoration. Its source of contamination is the cattle egret colony living on the mangrove island in the fishpond interior. The microbial abundance is therefore less influenced by increased freshwater flushing and the positive impact of increased water exchange and decreased residence time more apparent. Furthermore, phylogenetics of the three probes used in this study should to be taken into consideration: GenBac3 and Entero1a are phylogenetically very broad probes, targeting a diverse clade of organisms that may contain unknown members with variable salinity tolerances, although cultured representatives of this group so far are primarily gut commensals of animals. In contrast, because GFC is targeting a more specific organism (Firmicutes in the order *Lactobacillales* [50]) with few environmental members it is reasonable to assume that the organisms targeted by the assay have a different potential to tolerate salinity. The storm event revealed significantly increased concentrations of *Bacteroidales* and *Enterococcus* compared to baseline/non-storm sampling events, highlighting terrigenous freshwater runoff as the primary source of these microbes to the fishpond. The bird specific *Fusobacterium* showed no significant change in abundance between storm and baseline/non-storm conditions, supporting the hypothesis that the primary source of contamination is the cattle egret colony at the fishpond, which is independent of fresh water runoff. Taken together, the pattern of decreasing *Fusobacter*ia and consistent abundance of *Bacteroidales* and *Enterococcus* between the pre- and post-repair periods is intriguing, and may be related to differential environmental reservoirs of the two clades targeted by the assays. Certainly, microbial source tracking is a promising avenue to pursue further in order to understand how restoration and changes in circulation relate to

microbiological water quality assessments in traditional aquaculture systems generally and Hawaiian fishponds specifically.

5. CONCLUSIONS AND FUTURE IMPLICATIONS

Our physical measurements reveal that restoration regimes shifted the spatial distribution of relative water flux into and out of the fishpond with OM1 and *Kaho'okele* facilitating ~80% of water exchange together, making the northeastern portion the best flushed area of the fishpond. Similarly as before restoration, the remaining mākāhā (OM2, TM, RM2, RM3) together account for less than 20% of flux. Furthermore, restoration resulted in a ~5% increase of water exchanged during spring tide and ~16% increase of water exchange during neap tide. As a result, estimated minimum residence times decreased from 38 hours pre-restoration to 32 hours in post-restoration and maximum residence times decreased from 102 hours pre-restoration to 64 hours post-restoration work.

Repairing the wall restored the fishpond to its traditional nature: A loko kuapā - a seashore fishpond with an artificial stone wall enclosing the system during all tidal states and sluice gates facilitating rigorous water exchange. Increased periods of fish mortality caused by inhibited water exchange and resulting hypoxia could be avoided in the future by moving fish pens strategically to the eastern region of the fishpond (close to OM1 and *Kaho'okele*), which exhibits the highest flushing rates and presents favorable conditions for fish to thrive. Generally, understanding the physical environment of He'eia Fishpond will advance our knowledge of the dynamic biochemical and physical interactions in Hawaiian estuarine ecosystems.

Increased river flushing as a consequence of mangrove removal around the northern fishpond periphery caused a freshening of the fishpond post-restoration. Increased freshwater and nutrient input may be beneficial for native limu to thrive, which is the primary food source for the herbivorous target fish species in the fishpond, highlighting the advantage of management practices targeting the removal of invasive mangroves.

The decrease of bird specific *Fusobacteria* abundance from pre-to post-restoration suggests that increased flushing and decreased residence times had a positive impact on water quality. As the cattle egret colony on the mangrove island is the primary source of bird fecal contamination to the fishpond, removing the mangrove island is expected to reduce the amount of microbial

contamination from bird feces further. Despite increased flushing rates, we could not determine a significant decrease in abundance of *Bacterioidales* and *Enterococcus* pre- vs. post-restoration. As these microbes are introduced via terrigenous freshwater runoff, the increase in river flushing detected post-restoration, may increase abundance of such microbes in the fishpond in the future rendering need for pollution reduction management upstream.

Coastal and terrigenous environments are highly interconnected; the fishpond is an indicator of the health of the entire ahupua‘a. In order to improve water quality at the fishpond further, it is therefore important to approach management holistically taking the interconnectedness of the ahupua‘a carefully into consideration when managing restoration. Overall, this study clearly demonstrates the positive impact restoration regimes had on various physical and microbiological components of the fishpond ecosystem. Our results are encouraging and indicate that there is a significant potential for community-based restoration to revitalize this culturally and economically significant site for sustainable aquaculture in the future.

6. REFERENCES

1. Brooks, Mark. 1991. He‘eia Fishpond. Pp. 20-24 in Wyban, Carol A. (ed.) *Proceedings of The Governor’s Moloka‘i Fishpond Restoration Workshop*. Honolulu: Office of Hawaiian Affairs.
2. Kikuchi, W. K. Prehistoric Hawaiian Fishponds. *Science (80-.).* **1976**, *193*, 295–299, doi:10.1126/science.193.4250.295.
3. Kelly, M., & Kamehameha Schools/Bernice Pauahi Bishop Estate. (1973). *Some legendary and historical aspects of Heeia Fishpond, Koolau, Oahu*. Honolulu]: Dept. of Anthropology, Bernice P. Bishop Museum.
4. Allen, J. (1992). *Farming in Hawaii from Colonization to Contact: Radiocarbon Chronology and Implications for Cultural Change.,* New Zealand journal of archaeology.
5. Costa-Pierce, B., & American Institute of Biological Sciences. (1987). *Aquaculture in ancient Hawaii : Integrated farming systems included massive freshwater and seawater fish ponds; reprinted from BioScience, vol. 37, no. 5*. Washington, DC: American Institute of Biological Sciences.
6. Jokiel, P. L.; Rodgers, K. S.; Walsh, W. J.; Polhemus, D. A.; Wilhelm, T. A. Marine Resource Management in the Hawaiian Archipelago : The Traditional Hawaiian System in Relation to the Western Approach. **2011**, *2011*, doi:10.1155/2011/151682.
7. McGregor, D. Nā Kua‘āina: Living Hawaiian culture. Bishop Museum Press, Honolulu. **2007**.
8. Handy, E. S. C., and E. G. Handy. 1972. Native planters in old Hawaii: Their life, lore, and environment. Bernice P. Bishop Mus. Bull. 233
9. Keala, G., Hollyer, J.R., Castro, L., 2007. Loko I‘a: A manual on Hawaiian fishpond restoration and management. College of Tropical Agriculture and Human Resources, University of Hawaii, Honolulu, 76 pp.
10. Cobb, J. (1905). *The commercial fisheries of the Hawaiian Islands in 1903* ([U.S. Bureau of fisheries. Doc. no.590]). Washington: U.S. Govt. Print. Off.
11. Chimner, R. A.; Fry, B.; Kaneshiro, M. Y.; Cormier, N. Current Extent and Historical Expansion of Introduced Mangroves on O’ahu, Hawai’i. *Pacific Sci.* **2006**, *60*, 377–384, doi:10.1353/psc.2006.0013.

12. Gedan, K. B.; Kirwan, M. L.; Wolanski, E.; Barbier, E. B.; Silliman, B. R. The present and future role of coastal wetland vegetation in protecting shorelines: answering recent challenges to the paradigm. *Clim. Change* **2011**, *106*, 7–29, doi:10.1007/s10584-010-0003-7.
13. Twilley, R. W.; Lugo, A. E.; Patterson-Zucca, C. Litter Production and Turnover in Basin Mangrove Forests in Southwest Florida. *Ecology* **1986**, *67*, 670–683, doi:10.2307/1937691.
14. Crooks, J. (2002). Characterizing ecosystem-level consequences of biological invasions: The role of ecosystem engineers. *Oikos, 97*(2), 153-166.
15. Allen, J. A. Mangroves as Alien Species: The Case of Hawaii. *Glob. Ecol. Biogeogr. Lett.* **1998**, *7*, 61, doi:10.2307/2997698.
16. Demopoulos, Amanda W. J. (n.d.). *Aliens in Paradise a Comparative Assessment of Introduced and Native Mangrove Benthic Community Composition, Food-web Structure, and Litter-fall Production*.
17. Mccoy, D.; Mcmanus, M. A.; Hi, A.; Young, C.; Andrea, B. D.; Ruttenberg, K. C.; Alegado, A. Large-scale climatic effects on traditional Hawaiian fishpond aquaculture. **2017**, 1–17.
18. Young, C. W. (2011). Perturbation of nutrient inventories and phytoplankton community composition during storm events in a tropical coastal system; He‘eia Fishpond, O‘ahu, Hawai‘i. MS Thesis, Unviersity of Hawai‘i at Manoa, 425 pp.
19. Timmerman, A. H. V; Young, C.; Andrea, B. D.; Margaret, A. Dynamics of land-ocean linkages in a semi-enclosed tropical coastal system. 1–26. (in prep.)
20. Scott, T. M.; Rose, J. B.; Jenkins, T. M.; Farrah, S. R. Microbial Source Tracking : Current Methodology and Future Directions †. **2002**, *68*, 5796–5803, doi:10.1128/AEM.68.12.5796.
21. Kirs, M.; Kisand, V.; Wong, M.; Caffaro-Filho, R. A.; Moravcik, P.; Harwood, V. J.; Yoneyama, B.; Fujioka, R. S. Multiple lines of evidence to identify sewage as the cause of water quality impairment in an urbanized tropical watershed. *Water Res.* **2017**, *116*, 23–33, doi:10.1016/j.watres.2017.03.024.
22. Kelly, Marion. 1975. *Loko I‘a O He‘eia: Heeia Fishpond*. Honolulu: Bishop Museum.
23. Kleven, Coastal groundwater discharge as a source of nutrients to He‘eia fishpond, O‘ahu,

Hawai‘i. BSc Thesis, Unviersity of Hawai‘i at Manoa, 71 pp

24. Ringuet, S.; Mackenzie, F. T. Controls on nutrient and phytoplankton dynamics during normal flow and storm runoff conditions, southern Kaneohe Bay, Hawaii. *Estuaries* **2005**, *28*, 327–337, doi:10.1007/BF02693916.
25. Ostrander, C. E.; Mcmanus, M. A.; Decarlo, E. H.; Mackenzie, F. T. Temporal and Spatial Variability of Freshwater Plumes in a Semienclosed Estuarine–Bay System., doi:10.1007/s12237-007-9001-z.
26. Green, H. C.; Dick, L. K.; Gilpin, B.; Samadpour, M.; Field, K. G. Genetic Markers for Rapid PCR-Based Identification of Gull , Canada Goose , Duck , and Chicken Fecal Contamination in Water. **2012**, 503–510, doi:10.1128/AEM.05734-11.
27. Siefring, S.; Varma, M.; Atikovic, E.; Wymer, L.; Haugland, R. A. Improved real-time PCR assays for the detection of fecal indicator bacteria in surface waters with different instrument and reagent systems., doi:10.2166/wh.2008.022.
28. Dick, L. K.; Field, K. G. Rapid Estimation of Numbers of Fecal Bacteroidetes by Use of a Quantitative PCR Assay for 16S rRNA Genes. *Appl. Environ. Microbiol.* **2004**, *70*, 5695–5697, doi:10.1128/AEM.70.9.5695-5697.2004.
29. Haugland, R. A.; Siefring, S. C.; Wymer, L. J.; Brenner, K. P.; Dufour, A. P. Comparison of Enterococcus measurements in freshwater at two recreational beaches by quantitative polymerase chain reaction and membrane filter culture analysis. *Water Res.* **2005**, *39*, 559–568, doi:10.1016/j.watres.2004.11.011.
30. Ludwig, W.; Schleifer, K.-H. How Quantitative is Quantitative PCR with Respect to Cell Counts? *Syst. Appl. Microbiol.* **2000**, *23*, 556–562, doi:10.1016/S0723-2020(00)80030-2.
31. Sundararaghavan, H., Ertekin, Rifat Cengiz, & University of Hawaii at Manoa. Sea Grant College Program. (1997). *Tidal-jet redirection and temporal gate opening in a Hawaiian fishpond* (UNIHI-SEAGRANT-TR ; 97-01). Honolulu: University of Hawaii Sea Grant College Program.
32. Bathen, K. (1968). *A descriptive study of the physical oceanography of Kaneohe Bay, Oahu, Hawaii.* (Theses for the degree of Master of Science (University of Hawaii (Honolulu)). Oceanography ; no. 686). Honolulu]: Hawaii Institute of Marine Biology, University of Hawaii
33. Ertekin, R., Yang, Liqun, Sundararaghavan, H, & University of Hawaii at Manoa. Sea

Grant College Program. (1999). *Hawaiian fishpond studies : Web page development and the effect of runoff from the streams on tidal circulation* (UNIHI-SEAGRANT-TR ; 99-02). Honolulu, Hawaii: University of Hawaii at Manoa, School of Ocean and Earth Science and Technology : University of Hawaii Sea Grant College Program

34. Yang, L., & University of Hawaii at Manoa. Department of Ocean Engineering. (2000). *A circulation study of Hawaiian fishponds*.
35. Syvitski, J. P. M.; Milliman, J. D. Geology, Geography, and Humans Battle for Dominance over the Delivery of Fluvial Sediment to the Coastal Ocean. *J. Geol.* **2007**, *115*, 1–19, doi:10.1086/509246.
36. Milliman, J. D. Sediment discharge to the ocean from small mountainous rivers: The New Guinea example. *Geo-Marine Lett.* **1995**, *15*, 127–133, doi:10.1007/BF01204453.
37. Valle-Levinson, A. (2010). Estuarine salinity structure and circulation. In *Contemporary Issues in Estuarine Physics* (pp. 12-26). Cambridge: Cambridge University Press.
38. Ertekin, R., Sundararaghavan, H, Van Stiphout, A. T. F. M, & University of Hawaii at Manoa. Sea Grant College Program. (1996). *Moloka'i fishpond tidal circulation study* (UNIHI-SEAGRANT-TR ; 96-03). Honolulu: University of Hawaii Sea Grant College Program.
39. Siple, M. C.; Donahue, M. J. Journal of Experimental Marine Biology and Ecology Invasive mangrove removal and recovery : Food web effects across a chronosequence. *J. Exp. Mar. Bio. Ecol.* **2013**, *448*, 128–135, doi:10.1016/j.jembe.2013.06.008.
40. Scott, T. M.; Rose, J. B.; Jenkins, T. M.; Farrah, S. R.; Lukasik, J. Microbial source tracking: current methodology and future directions. *Appl. Environ. Microbiol.* **2002**, *68*, 5796–803, doi:10.1128/AEM.68.12.5796-5803.2002.
41. Shanks, O. C.; Kelty, C. A.; Sivaganesan, M.; Varma, M.; Haugland, R. A. Quantitative PCR for genetic markers of human fecal pollution. *Appl. Environ. Microbiol.* **2009**, *75*, 5507–13, doi:10.1128/AEM.00305-09.
42. Fleming, K., Keala, Graydon, & Monahan, William. (1995). *The economics of revitalizing Hawaiian fishpond production*(AgriBusiness (Honolulu, Hawaii) ; no. 9). Honolulu]: Cooperative Extension Service, Dept. of Agricultural and Resource Economics, University of Hawai'i at Mānoa.
43. Boehm, A. B.; Sassoubre, L. M. *Enterococci as Indicators of Environmental Fecal*

Contamination; Massachusetts Eye and Ear Infirmary, 2014

44. Noble, R. T.; Lee, I. M.; Schiff, K. C. Inactivation of indicator bacteria from various sources of fecal contamination in seawater and freshwater. Journal of Applied Microbiology, March 2004, Vol.96(3), pp.464-472
45. Ortega, C.; Solo-Gabriele, H. M.; Abdelzaher, A.; Wright, M.; Deng, Y.; Stark, L. M. Correlations between microbial indicators, pathogens, and environmental factors in a subtropical estuary. *Mar. Pollut. Bull.* **2009**, *58*, 1374–81, doi:10.1016/j.marpolbul.2009.04.015.
46. Shehane, S.; Harwood, V.; Whitlock, J.; Rose, J. The influence of rainfall on the incidence of microbial faecal indicators and the dominant sources of faecal pollution in a Florida river., doi:10.1111/j.1365-2672.2005.02554.x.
47. Islam, M. M. M.; Hofstra, N.; Islam, M. A. The Impact of Environmental Variables on Faecal Indicator Bacteria in the Betna River Basin, Bangladesh. *Environ. Process.* **2017**, *4*, 319–332, doi:10.1007/s40710-017-0239-6.
48. U.S. Environmental Protection Agency 1986. Ambient water quality criteria for bacteria—1986. EPA-440/5-84/002. U.S. Environmental Protection Agency, Office of Water, Washington, DC
49. Weigand, M. R.; Ryu, H.; Bozcek, L.; Konstantinidis, K. T.; Santo Domingo, J. W. Draft Genome Sequence of Catellicoccus marimammalium, a Novel Species Commonly Found in Gull Feces. *Genome Announc.* **2013**, *1*, doi:10.1128/genomeA.00019-12.
50. Sinigalliano, C. D.; Ervin, J. S.; Van De Werfhorst, L. C.; Badgley, B. D.; Ballesté, E.; Bartkowiak, J.; Boehm, A. B.; Byappanahalli, M.; Goodwin, K. D.; Gourmelon, M.; Griffith, J.; Holden, P. A.; Jay, J.; Layton, B.; Lee, C.; Lee, J.; Meijer, W. G.; Noble, R.; Raith, M.; Ryu, H.; Sadowsky, M. J.; Schriewer, A.; Wang, D.; Wanless, D.; Whitman, R.; Wuertz, S.; Santo Domingo, J. W. Multi-laboratory evaluations of the performance of Catellicoccus marimammalium PCR assays developed to target gull fecal sources. *Water Res.* **2013**, *47*, 6883–6896, doi:10.1016/j.watres.2013.02.059.
51. Ryu, H.; Griffith, J. F.; Khan, I. U. H.; Hill, S.; Edge, T. A.; Toledo-hernandez, C.; Gonzalez-nieves, J. Comparison of Gull Feces-Specific Assays Targeting the 16S rRNA Genes of Catellicoccus marimammalium and Streptococcus spp . **2012**, 1909–1916, doi:10.1128/AEM.07192-11.

52. Lu, J.; Domingo, J. W. S.; Lamendella, R.; Edge, T.; Hill, S.; Al, L. U. E. T.; Icrobiol, A. P. P. L. E. N. M. Phylogenetic Diversity and Molecular Detection of Bacteria in Gull Feces. **2008**, *74*, 3969–3976, doi:10.1128/AEM.00019-08.

53. Cloutier, D. D.; Mclellan, S. L. crossm Distribution and Differential Survival of Traditional and Alternative Indicators of Fecal Pollution at Freshwater Beaches. **2017**, *83*, 1–16.

54. Lee, C.; Marion, J. W.; Lee, J. Science of the Total Environment Development and application of a quantitative PCR assay targeting Catellicoccus marimammalium for assessing gull-associated fecal contamination at Lake Erie beaches. *Sci. Total Environ.* **2013**, *454–455*, 1–8, doi:10.1016/j.scitotenv.2013.03.003.

7. TABLES

Table 1. Mākāhā dimensions and heading
Ocean Mākāhā 2 (Hīhīmanu); Ocean Break (Kahoʻokele); Ocean Mākāhā 2 (Mākāhā Nui); Triple Mākāhā (Kahoa Lāhui); River Mākāhā 3 (Wai 1); River Mākāhā 2 (Wai 2).

Mākāhā	Hawaiian name	Mākākā heading	Width (m)	Height (m)
Ocean Mākāhā 2 (OM2)	*Hīhīmanu*	111°/291°	2.00	1.24
Ocean Break (OB)	*Kahoʻokele*	80°/260°	3.05	1.75
Ocean Mākāhā 1 (OM1)	*Mākāhā Nui*	63°/243°	6.48	1.73
Triple Mākāhā 1 (TM1)	*Kahoa Lāhui*	48°/228°	1.88	1.19
Triple Mākāhā 2 (TM2)	*Kahoa Lāhui*	48°/228°	1.78	1.12
Triple Mākāhā 3 (TM3)	*Kahoa Lāhui*	48°/228°	1.55	1.07
River Mākāhā 3 (RM3)	*Wai 1*	310°/130°	2.18	1.47
River Mākāhā 2 (RM2)	*Wai 2*	290°/110°	1.85	1.73

Table 2. *In situ* instrumentation and rationale
I*n situ* instrumentation deployed in the present study with deployment specifications, location and sampling rationale. Shortages: T = temperature, S = Salinity, O2 =% DO saturation.

Instrumentation	Data Type	Sampling Frequency	Data Acquisition Frequency	Location	Rationale
Sontek Argonaut SW	Current direction and magnitude, pressure, temperature	7 day serial deployment	20 s	All mākāhā (RM2, RM3, TM, OM1, OB, OM2)	High frequency current data to quantify water movement into/out of makaha
Hobo Pressure Sensors	Pressure , temperature	10 day deployment	2 min	Stake 11	High frequency pressure data to monitor tidal variability in the pond interior
Wind gauge	Wind speed and direction	Serial long term deployment	6 min	HIMB (Moku o Loʻe)	Wind data used for a record of daily variability in wind direction and magnitude
Ultrasonic Tide gauge	Distance to water (Water level)	Serial long term deployment	2 min	HIMB (Moku o Loʻe)	High frequency water level data to monitor tidal variability at HIMB; tidal data was used for reference to asess temporal variability
Rain gauge	Local Precipitation	Serial long term deployment	15 min	NOAA Luluku Station (HI15)	Rainfall data used for a record of daily variability
Stream Discharge Gage	Stream discharge	Serial long term deployment	15 min	USGS Haʻiku Stream discharge station (Station #16275000)	Haʻiku Stream discharge variability used as an indicator of Heʻeia Stream discharge
YSI (ProPlus) multi-parameter water quality sonde	Temperature, salinity, O2, pH, fluorescence, turbidity	Monthly	Discrete	L01-L011, M01-M06,E01,E02	Evaluate water column stratification (T, S) and biogeochemical parameters (O2, pH, fluorescence, turbidity) at discrete sampling sites

Table 3. He‘eia Fishpond discrete sample site locations pre -and post-restoration
GPS coordinates are given for nineteen 2017 sampling stations: 6 Mākāhā: River Mākāhā 2 (M01), River Mākāhā 3 (M02), Triple Mākāhā (M03), Ocean Mākāhā 2 (M04), Ocean Break (M05), Ocean Mākāhā 2 (M06); 2 Endmembers: River (E01), Ocean (E02); 10 Locations in the pond interior: L01-L10; and 12 2014 sampling stations: 10 Locations in the pond interior (P1-P10) and two makāhā (M01 and M05).

Post-restoration			
Site name	**ID**	**Latitude**	**Longitude**
Location 01	L01	21.43257	-157.80704
Location 02	L02	21.4352681	-157.80803
Location 03	L03	21.4366529	-157.80833
Location 04	L04	21.436895	-157.80736
Location 05	L05	21.438975	-157.80939
Location 06	L06	21.4370507	-157.81026
Location 07	L07	21.4373252	-157.81085
Location 08	L08	21.4377307	-157.80979
Location 09	L09	21.436953	-157.80979
Location 10	L10	21.4360941	-157.80661
Location 11	L11	21.4379231	-157.80782
River Mākāhā 2	M01	21.4379231	-157.80782
River Mākāhā 1	M02	21.4386583	-157.81077
Triple Mākāhā	M03	21.4396667	-157.80993
Ocean Mākāhā 1	M04	21.4384222	-157.80675
Ocean Break	M05	21.4372333	-157.80583
Ocean Mākāhā 2	M06	21.4357389	-157.80531
River Endmember	E01	21.4338861	-157.80528
Ocean Endmember	E02	21.4412083	-157.80616
Pre-restoration			
Site name	**ID**	**Latitude**	**Longitude**
Location 01	P01	21.43272	-157.80746
Location 02	P02	21.4347	-157.80862
Location 03	P03	21.43743	-157.81073
Location 04	P04	21.43871	-157.81001
Location 05	P05	21.43703	-157.80923
Location 06	P06	21.43573	-157.80754
Location 07	P07	21.439924	-157.80829
Location 08	P08	21.43769	-157.80676
Location 09	P09	21.43579	-157.80563
Location 10	P10	21.43353	-157.80646
River Mākāhā 2	M01	21.4379231	-157.80782
Ocean Break	M05	21.4372333	-157.80583

Table 4. Sampling timeline
Sontek Argonaut SW flow meters were deployed for a minimum of 7 days at each of the six mākāhā channel. YSI and discrete water sampling was done on three sampling events pre- and post-restoration respectively.

Pre vs. post - restoration	Instrumentation	Location ID	Hawaiian name	Deployment period (dd/mm/yyyy)	Sampling period (in days)
Pre-restoration	Sontek Argonaut SW	OM2	*Hihimanu*	01/21/2012-01/28/2012	7
Pre-restoration	Sontek Argonaut SW	OB	Kahoʻokele	5/5/2012	1
Pre-restoration	Sontek Argonaut SW	OM1	*Nui*	04/07/2012-04/12/2012	5
Pre-restoration	Sontek Argonaut SW	TM	*Kahoalahui*	05/04/2012-05/05/2012	2
Pre-restoration	Sontek Argonaut SW	RM3	*Wai 1*	4/26/2012	1
Pre-restoration	Sontek Argonaut SW	RM2	*Wai 2*	4/26/2012-05/01/2012	5
Pre-restoration	YSI sonde, discrete water sampling	P1-P10, M01-M06	na	8/28/2014	1
Pre-restoration	YSI sonde, discrete water sampling	P1-P10, M01-M07	na	9/11/2014	1
Pre-restoration	YSI sonde, discrete water sampling	P1-P10, M01-M08	na	10/23/2014	1
Ocean Break Repair				2015	
Post-restoration	Sontek Argonaut SW	OM2	*Hihimanu*	03/31/2018-04/07/2018	7
Post-restoration	Sontek Argonaut SW	OB	Kahoʻokele	03/10/2018-03/17/2018	7
Post-restoration	Sontek Argonaut SW	OM1	*Nui*	03/31/2018-04/07/2018	7
Post-restoration	Sontek Argonaut SW	TM	*Kahoalahui*	03/31/2018-04/07/2018	7
Post-restoration	Sontek Argonaut SW	RM3	*Wai 1*	04/07/2018-04/15/2018	7
Post-restoration	Sontek Argonaut SW	RM2	*Wai 2*	04/07/2018-04/15/2018	7
Post-restoration	YSI sonde, discrete water sampling	M01-M06, E01-E02, M01-M06	*na*	2/18/2017	1
Post-restoration	YSI sonde, discrete water sampling	M01-M06, E01-E02, M01-M07	*na*	4/2/2017	1
Post-restoration	YSI sonde, discrete water sampling	M01-M06, E01-E02, M01-M08	*na*	6/2/2017	1

Table 5. Sontek Argonaut SW instrument specifications
Further instruments specifications can be found at https://eng.ucmerced.edu.

Instrument Type	Argonaut SW Current Profiler
Manufacturer	Sontek
Capabilities	2-D velocity measurement (using 2 acoustic beams) along channel and vertical velocity components; water level measurement using vertical acoustic beam; temperature
Velocity Profiling Range	Maximum Depth: 5.0m (16ft); Minimum Depth: 0.3m (1ft)
Water Level Range	Minimum Depth: above transducer: 0.10m (0.3ft), total water depth: 0.20m (0.6ft); Maximum depth: 5.0m (16ft)
Accuracy	Velocity: 1% of measured value ± 0.5 cm/s; water level: ±0.1% of measured level, ±0.3cm (0.01ft)
Inventory	3
Sampling Frequency	900 Hz

Table 6. List of primers tested
List of 8 primers targeting the 16S gene of *Catellicoccus marimammalium* that had been detected in fecal contamination from gulls in coastal environment. In addition, primers targeting *Enterococcus* and *Bacteroidales* are listed.

Assay Name	Oligo Name	Sequence 5'-3'	Source	Target length	Reference
Gull2Taqman	Gull2f	TGCATCGACCTAAAGTTTTGAG	Gull	412bp	(Sinigalliano et al., 2010)
Gull2Taqman	Gull2r	[6FAM]-CTGAGAGGGTGATCGGCCACATTGGGACT-	Gull	412bp	(Sinigalliano et al., 2010)
Gull2Taqman	Gull2p	*[BHQ1]*	Gull	412bp	(Sinigalliano et al., 2010)
LeeSeaGull	CaT#998F	AGGTGCTAATACCGCATAATACAGAG	Gull	112bp	(Lee et al. 2012)
LeeSeaGull	CaT#998R	GCCGTTACCTCACCGTCTA	Gull	112bp	(Lee et al. 2012)
LeeSeaGull	CaT#998P	[6FAM]-TTCTCTGTTGAAAGGCGCTT-[MGB]	Gull	112bp	(Lee et al. 2012)
GFC-Catellicoccus marimammalium	GFC	CCC TTG TCG TTA GTT GCC ATC ATT C	Gull	162bp	(Green et al. 2012)
GFC-Catellicoccus marimammalium	GFC	GCC CTC GCG AGT TCG CTG C	Gull	162bp	(Green et al. 2012)
GFB-Unclassified Fusobacterium spp	GFB	TCA TGA AAG CTA TAT GCG CCA AAA	Gull	176bp	(Green et al. 2012)
GFB-Unclassified Fusobacterium spp	GFB	TCC ATT GTC CAA TAT TCC CCA C	Gull	176bp	(Green et al. 2012)
GFD Unclassified Helicobacter spp.	GFD	TCG GCT GAG CAC TCT AGG G	Gull	123bp	(Green et al. 2012)
GFD Unclassified Helicobacter spp.	GFD	GCG TCT CTT TGT ACA TCC CA	Gull	123bp	(Green et al. 2012)
gull3 SYBR green	gull3	SAG1F: ATTTAACCCATGTTAGATGC	Gull	319bp	(Ryu et al. 2012)
gull3 SYBR green	gull3	SAG1R: CGTCCCTTTCTGGTAAGT	Gull	319bp	(Ryu et al. 2012)
gull4 TaqMan	gull4	qGull7F: CTTGCATCGACCTAAAGTTTTGAG	Gull	116bp	(Ryu et al. 2012)
gull4 TaqMan	gull4	qGull8R: GGTTCTCTGTATTATGCGGTATTAGCA	Gull	116bp	(Ryu et al. 2012)
gull4 TaqMan	gull4	ıll7Pb: FAM-ACACGTGGGTAACCTGCCCATCAGA-TAM	Gull	116bp	(Ryu et al. 2012)
Enteroccocus	Entero1af	AGAAATTCCAAACGAACTTG	na	na	na
Enteroccocus	Entero1ar	CAGTGCTCTACCTCCATCATT	na	na	na
Enteroccocus	Entero1ap	[™/TGGTTCTCT/ZEN™/CCGAAATAGCTTTAGGGCTA/I	na	na	na
Bacteroidales	GenBac3f	GGGGTTCTGAGAGGAAGGT	na	na	na
Bacteroidales	GenBac3r	CCGTCATCCTTCACGCTACT	na	na	na
Bacteroidales	GenBac3p	M™/CAATATTCC/ZEN™/TCACTGCTGCCTCCCGTA/IB(	na	na	na

Table 7. Results of PCR analysis
8 primers targeting the 16S gene of *Catellicoccus marimammalium* and two broad spectrum primers targeting *Bacteroidales* (GenBac3) and *Enteroccocus* (Entero1a) were tested with PCR analysis on cattle egret feces extracted DNA.

Pos	Name	Ct SYBR
A1	Gull2: BF 1	
A2	Gull2: BF 2	
A3	Gull2: Neg	
A4	Cat#998: BF 1	
A5	Cat#998: BF 2	
A6	Cat#998: Neg	
A7	GFC: BF 1	27.81
A8	GFC: BF 2	25.50
A9	GFC: Neg	
A10	GFB: BF 1	
A11	GFB: BF 2	
A12	GFB: Neg	
B1	GFD: BF 1	26.19
B2	GFD: BF 2	
B3	GFD: Neg	
B4	Gull3: BF 1	
B5	Gull3: BF 2	
B6	Gull31: Neg	
B7	Gull4: BF 1	
B8	Gull4: BF 2	
B9	Gull4: Neg	
B10	GenBac3: Bird Poop 1	24.98
B11	GenBac3: Bird Poop 2	26.91
B12	GenBac3: Neg	
C1	Entero1A: Bird Poop 1	17.44
C2	Entero1A: Bird Poop 2	18.37
C3	Entero1A: Neg	
C4	GenBac3: B Positive Control	24.78
C5	Entero1A: F Positive Control	25.60

Table 8. Flux measurement meteorological conditions pre- and post-restoration
Daily and cumulative rainfall from NOAA's Luluku station (HI15), Ha'iku Stream discharge from USGS Stream Gauge, tidal and wind data from HIMB's weather station (see section 2.1. for more detail).

Location	Date	Daily Rainfall (cm)	Cumulative rainfall 4 days ahead of sampling event (cm)	Mean Hai'ku Stream Discharge (m3/s) over 24 hrs	Rainfall over Storm Threshold	Tide	Wind direction	Wind magnitude (in knots)
RM2	4/26/2012	1.3	2.08	0.07	N	Neap	E	10
RM3	4/26/2012	1.3	2.08	0.07	N	Neap	E	10
TM	5/4/2012	0.28	0.99	0.05	N	Spring	NE	12
OM1	4/9/2012	1.32	2.34	0.07	N	Spring	NE	13
OB	5/5/2012	0.3	1.29	0.05	N	Spring	NE	11
OM2	1/22/2012	0.05	0.1	0.04	N	Spring	NE	10
RM2	4/15/2018	1.9	6.35	0.09	N	Spring	NE	11
RM3	4/14/2018	1.11	5.71	0.08	N	Spring	NE	11
TM	3/31/2018	0.64	0.64	0.06	N	Spring	NE	5
OM1	3/31/2018	0.64	0.64	0.06	N	Spring	NE	5
OB	3/15/2018	0	6.35	0.07	N	Spring	NE	5
OM2	4/1/2018	0	0.64	0.06	N	Spring	NE	3
RM2	4/8/2018-04/09/2018	1.65	6.35	0.16	N	Neap	N	7
RM3	4/07/2018-04/08/2018	1.52	7	0.09	N	Neap	NE	4
TM	04/06/2018-04/07/2018	2.29	6.1	0.08	N	Neap	NE	9
OM1	04/06/2018-04/07/2018	2.29	6.1	0.08	N	Neap	NE	9
OB	03/08/2018-03/09/2018	0.5	0.5	0.11	N	Neap	NE	13
OM2	04/06/2018-04/07/2018	2.29	6.1	0.08	N	Neap	NE	9

Table 9. YSI and discrete sampling meteorological conditions pre- and post-restoration
Daily and cumulative rainfall from NOAA's Luluku station (HI15), Ha'iku Stream discharge from USGS Stream Gauge, tidal and wind data from HIMB's weather station (see section 2.1. for more detail). <5.1cm/24 hours is considered baseline (non-storm) conditions.

Date	Event	Daily Rainfall (cm)	Cumulative rainfall 4 days ahead of sampling event (cm)	Mean Hai'ku Stream Discharge (m3/s) over 24 hrs	Rainfall over Storm Threshold	Tide	Rising or dropping	Wind direction	Wind magnitude (in knots)
2/18/2017	1	0.46	38,1	0.07	N	Neap Low	Slack	NNE	3
4/2/2017	2	0	1.54	0.06	N	Neap Low	Dropping	E	6
6/2/2017	3	0.91	45.72	na	N	Neap Low	Dropping	E	6
8/28/2014	4	0.61	37.8	0.06	N	Neap Low	Slack	NE	4
9/11/2014	5	0	3.35	0.05	N	Intermediate	Slack	E	4
10/23/2014	6	42.3	101.5	0.4	Y (Storm Ana)	Spring Low	Slack	E	5

Table 10. Post-restoration site-specific mean, max and total water volume flux
Site specific mean, max, total water volume flux over entire tidal cycle, length of individual tidal cycles and flux per hour rates are given for spring flood, spring ebb, neap flood and neap ebb tides.

Site	Year	Tide	Mean. (m^3 s-1)	Max (m^3 s-1)	Length of the cycle (in hrs)	Cumulative flux over entire tidal cycle	Flux per hour
Spring Flood						Total= 191660	31778
RM2	2018	Spring Flood	0.05	0.16	4.43	840	190
RM3	2018	Spring Flood	0.40	0.93	4.55	7140	1569
TM	2018	Spring Flood	1.47	0.92	4.36	24420	5601
OM1	2018	Spring Flood	4.18	9.70	6.29	97800	15548
OB	2018	Spring Flood	2.02	4.69	7.29	54380	7460
OM2	2018	Spring Flood	0.39	0.95	5.02	7080	1410
Spring Ebb						Total= -174880	-30851
RM2	2018	Spring Ebb	0.07	-0.09	5.50	1560	284
RM3	2018	Spring Ebb	-0.32	-0.63	6.32	-7600	-1203
TM	2018	Spring Ebb	-0.87	-0.62	6.31	-20220	-3204
OM1	2018	Spring Ebb	-3.60	-4.86	5.53	-76320	-13801
OB	2018	Spring Ebb	-1.10	-3.12	5.50	-67520	-12276
OM2	2018	Spring Ebb	-0.17	-0.43	7.35	-4780	-650
Neap Flood						Total= 141384	16717
RM2	2018	Neap Flood	0.05	0.20	7.41	1300	175
RM3	2018	Neap Flood	0.32	0.98	8.29	9720	1172
TM	2018	Neap Flood	0.51	0.36	7.31	13620	1863
OM1	2018	Neap Flood	2.26	5.41	9.46	78744	8324
OB	2018	Neap Flood	1.35	2.52	7.30	36440	4992
OM2	2018	Neap Flood	0.05	0.24	8.20	1560	190
Neap Ebb						Total= -159938	-10584
RM2	2018	Neap Ebb	0.88	-0.09	17.46	5640	323
RM3	2018	Neap Ebb	-0.17	-0.57	15.50	-9880	-637
TM	2018	Neap Ebb	-0.30	-0.30	15.50	-17100	-1103
OM1	2018	Neap Ebb	-1.60	-3.19	14.09	-81298	-5770
OB	2018	Neap Ebb	-0.86	-1.80	17.10	-53280	-3116
OM2	2018	Neap Ebb	-0.08	-0.25	14.34	-4020	-280

Table 11. Post-restoration relative mākāhā flux rates
Site-specific volume of water exchanged during one tidal cycle. In parentheses is the relative magnitude of each flow rate, represented as percent of the total flux measured for all locations, during each tidal cycle. Positive values represent water flowing into the He‘eia Fishpond during flood tide. Negative values represent water flowing out of He‘eia Fishpond or into Kāne‘ohe Bay during ebb tide.

Site	Spring Flood	Spring Ebb	Neap Flood	Neap Ebb
RM2 *(Wai 2)*	**840** (0.44%)	**1560** (−0.89%)	**1300** (0.92%)	**5640** (−3.53%)
RM3 *(Wai 1)*	**7140** (3.37%)	**−7600** (4.35%)	**9720** (6.87%)	**−9880** (6.18%)
TM *(Kahoa Lāhui)*	**24420** (12.74%)	**−20220** (11.56%)	**13620** (9.63%)	**−17100** (10.69%)
OM1 *(Mākāhā Nui)*	**97800** (51.03%)	**−76320** (43.64%)	**78744** (55.7%)	**−81298** (50.83%)
OB *(Kaho‘okele)*	**54380** (28.37%)	**−67520** (38.61%)	**36440** (25.77%)	**−53280** (33.31%)
OM2 *(Hīhīmanu)*	**7080** (3.69%)	**−4780** (2.73%)	**1560** (1.1%)	**−4020** (2.51%)
Mākāhā Flow Rate Total	**191660** (100%)	**−174880** (100%)	**141384** (100%)	**−159938** (100%)

Table 12. Fishpond volumes pre- and post-restoration
Fishpond volumes for four tidal states calculated based on bathymetry data pre-restoration and post-restoration.

Time	Spring Low	Spring High	Neap Low	Neap High
Pre-restoration	64.070	282.720	78.050	133.890
Post-restoration	48.060	264.730	63.160	149.550

Table 13. Fishpond water exchange rates pre- and post-restoration
Water exchange rates pre- and post-restoration for spring and neap tide respectively and percentage increase in water exchange.

Year	Pre-restoration	Post-restoration	**% increase in water exchange**
Spring Tide	77.34%	81.85%	**4.51%**
Neap Tide	41.71%	57.77%	**16.06%**

Table 14. Pre-restoration site-specific mean, max and total water volume flux
Site specific mean, max, total water volume flux over entire tidal cycle, length of individual tidal cycles and flux per hour rates are given for spring flood, spring ebb, neap flood and neap ebb tides.

Site	Year	Tide	Mean. (m^3 s-1)	Max (m^3 s-1)	Length of the cycle (in hrs)	Cumulative flux over entire tidal cycle (m^3)	Flux per hour (m^3)
Neap Flood						Total= 241413	55112
RM2	2012	Spring Flood	0.09	0.23	6.22	2057	331
RM3	2012	Spring Flood	0.09	0.28	6.46	2249	348
Spring Flood							
TM	2012	Spring Flood	0.58	0.94	2.10	4106	1955
OM1	2012	Spring Flood	1.75	4.27	4.56	31101	6820
OB	2012	Spring Flood	11.53	31.54	4.45	197820	44454
OM2	2012	Spring Flood	0.28	0.58	3.39	4081	1204
Neap Ebb						Total=-241685	-57441
RM2	2012	Spring Ebb	-0.09	-0.2	17.52	-5515	-315
RM3	2012	Spring Ebb	-0.1	-0.34	16.30	-5791	-355
Spring Ebb							
TM	2012	Spring Ebb	-0.233	-0.48	6.54	-5802	-887
OM1	2012	Spring Ebb	-0.5	-1.83	19.54	-26886	-1376
OB	2012	Spring Ebb	-13.55	-30.84	3.56	-192780	-54152
OM2	2012	Spring Ebb	-0.13	-0.41	13.80	-4912	-356

Table 15. Pre -and post-restoration relative mākāhā flux rate comparison
Comparison of site-specific volume of water exchanged during flood and ebb tidal cycles pre-restoration (2012) vs. post-restoration (2018). In parentheses is the relative magnitude of each flow rate, represented as percent of the total flux measured for all locations, during each tidal cycle. Positive values represent water flowing into the He‘eia Fishpond during flood tide. Negative values represent water flowing out of He‘eia Fishpond or into Kāne‘ohe Bay during ebb tide.

	Flood		**Ebb**	
Site	**Pre-restoration**	**Post-restoration**	**Pre-restoration**	**Post-restoration**
RM2 *(Wai 2)*	**2057** (0.85%)	**1300** (0.67%)	**−5515** (2.28%)	**5640** (−3.25%)
RM3 *(Wai 1)*	**2249** (0.93%)	**9720** (5.1%)	**−5791** (2.4%)	**−9880** (5.7%)
TM *(Kahoa Lāhui)*	**4106** (1.71%)	**24420** (12.54%)	**−5802** (2.41%)	**−20220** (11.68%)
OM1 *(Mākāhā Nui)*	**31101** (12.88%)	**97800** (50.24%)	**−26886** (11.12%)	**−76320** (44.1%)
OB. *(Kaho‘okele)*	**197820** (81.94%)	**54380** (27.93%)	**−192780** (79.76%)	**−67520** (39.01%)
OM2 *(Hīhīmanu)*	**4081** (1.69%)	**7080** (3.61%)	**−4912** (2.03%)	**−4780** (2.76%)
Mākāhā Flow Rate Total	**241413** (100%)	**194700** (100%)	**−241685** (100%)	**−173080** (100%)

8. FIGURES

Figure 1. Mangrove removal chronosequence
Dates of successive mangrove removal efforts are shown, as are areas scheduled for future mangrove removal. The mākāhā (sluice gates) and kuapā (wall) are shown for reference.

Figure 2. He'eia ahupua'a location
The island of Oahu with He'eia watershed on its windward site. He'eia fishpond is located at the terminus of the ahupua'a adjacent to Kāne'ohe Bay (photo credit: The Nature Conservancy).

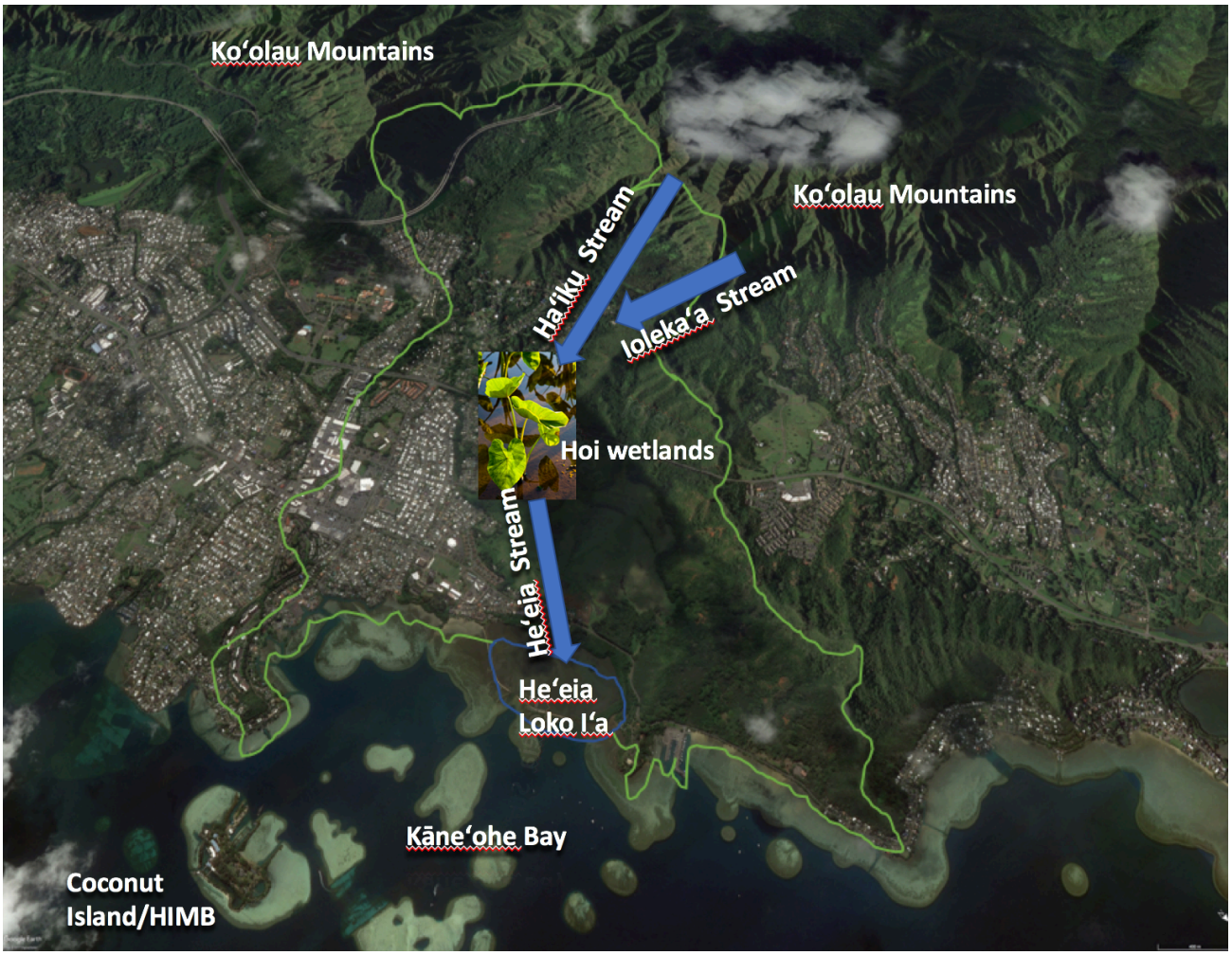

Figure 3. He'eia ahupua'a
The area of Heʻeia watershed is outlined in green and Heʻeia fishpond in blue. Heʻeia Stream originates as Haʻikū Stream near the ridgeline of the Koʻolau Mountains and converges with Iolekaʻa Stream before entering Heʻeia wetlands (Kākoʻoʻōiwi) and then flowing past Heʻeia Fishpond into Kāneʻohe Bay.

Figure 4. Fishpond kuapā
Picture of the wall (*kuapā*) that forms a complete circle (2.5 km) around the pond. The wall is built from two parallel volcanic rock walls that are filled with fossilized coral rock rubble.

Figure 5. Mākāhā
a) Ocean Mākāhā 2 (*Hīhīmanu*); b) Ocean Break (K*aho'okele*); c) Ocean Mākāhā 2 (*Mākāhā Nui*); d) Triple Mākāhā (*Kahoa Lāhui*); e) River Mākāhā 3 (*Wai 1*); f) River Mākāhā 2 (*Wai 2*).

Figure 6. Map of mākāhā locations and names
He'eia coastal ocean observing system mākāhā names are in white, Hawaiian mākāhā names (used by *Paepae o He'eia*) are in yellow.

Figure 7. Mākāhā grid types
Top: Mākāhā grid constructed from wood; Bottom: Mākāhā grid constructed from plastic.

Figure 8. Luluku (HI15) rain gauge and HIMB weather station location
Location of Luluku rain gauge and HIMB weather station relative to He'eia fishpond.

Figure 9. Map of post-restoration He‘eia Fishpond discrete sample site locations
6 Mākāhā: River Mākāhā 2 (M01), River Mākāhā 3 (M02), Triple Mākāhā (M03), Ocean Mākāhā 1 (M04), Ocean Break (M05), Ocean Mākāhā 2 (M06); 2 Endmembers: River (E01), Ocean (E02); 10 Locations in the pond interior: L01-L10.

Figure 10. Flow meter deployment set-up
Pictures depicting the Nortek Aquadopp current meter deployment set-up. Note: For this study, only data from the Sontek Argonaut current meter was utilized.

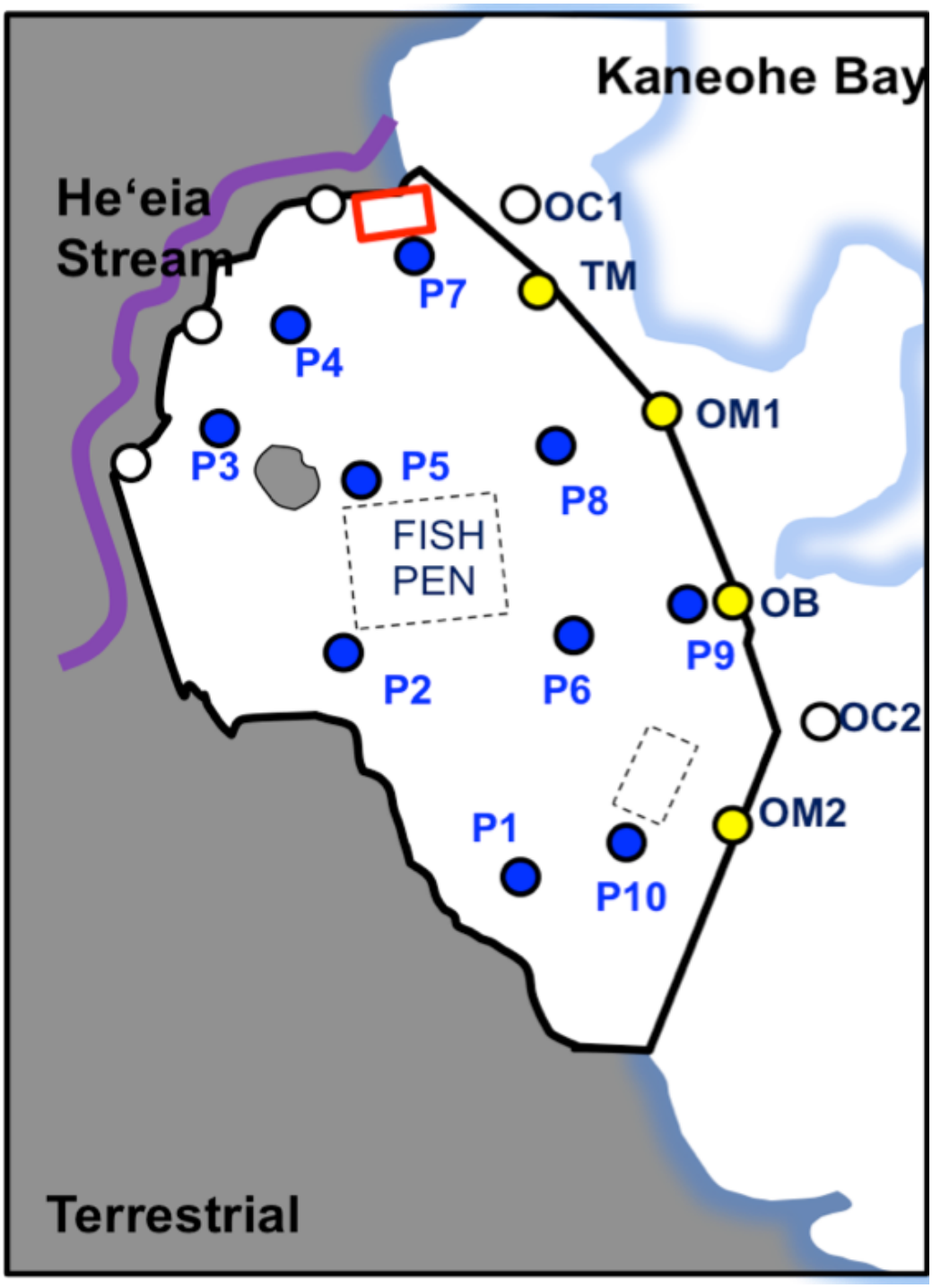

Figure 11: Map of pre-restoration He'eia Fishpond discrete sample site locations
4 Mākāhā: Triple Mākāhā (TM), Ocean Mākāhā 1 (OM1), Ocean Break (OB), Ocean Mākāhā 2 (OM2); 2 Endmembers: Ocean 1 (OC1) and Ocean 2 (OC2); 10 Locations in the pond interior: P1-P10.

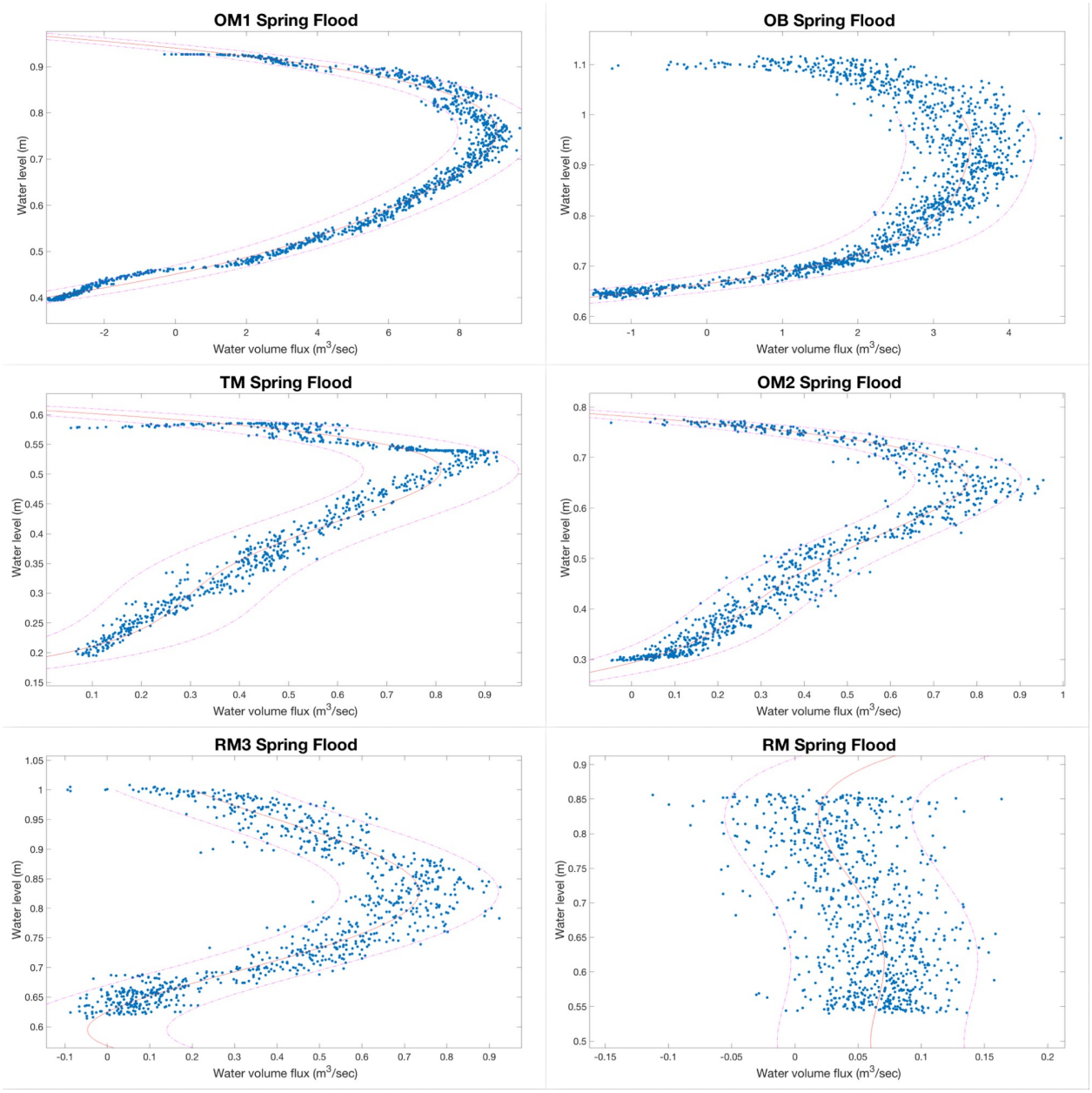

Figure 12. Site specific spring flood rating curves post-restoration
Water volume flux (m^3 s^{-1}) relative to the water level (m) for all 6 makāha during spring flood tide. A positive water volume flux represents flux into the fishpond from Kaneʻohe Bay or Heʻeia Stream. A negative water volume flux represents flux out of the fishpond into Kaneʻohe Bay. Note the different flux (m^3 s^{-1}) scales on the x-axes.

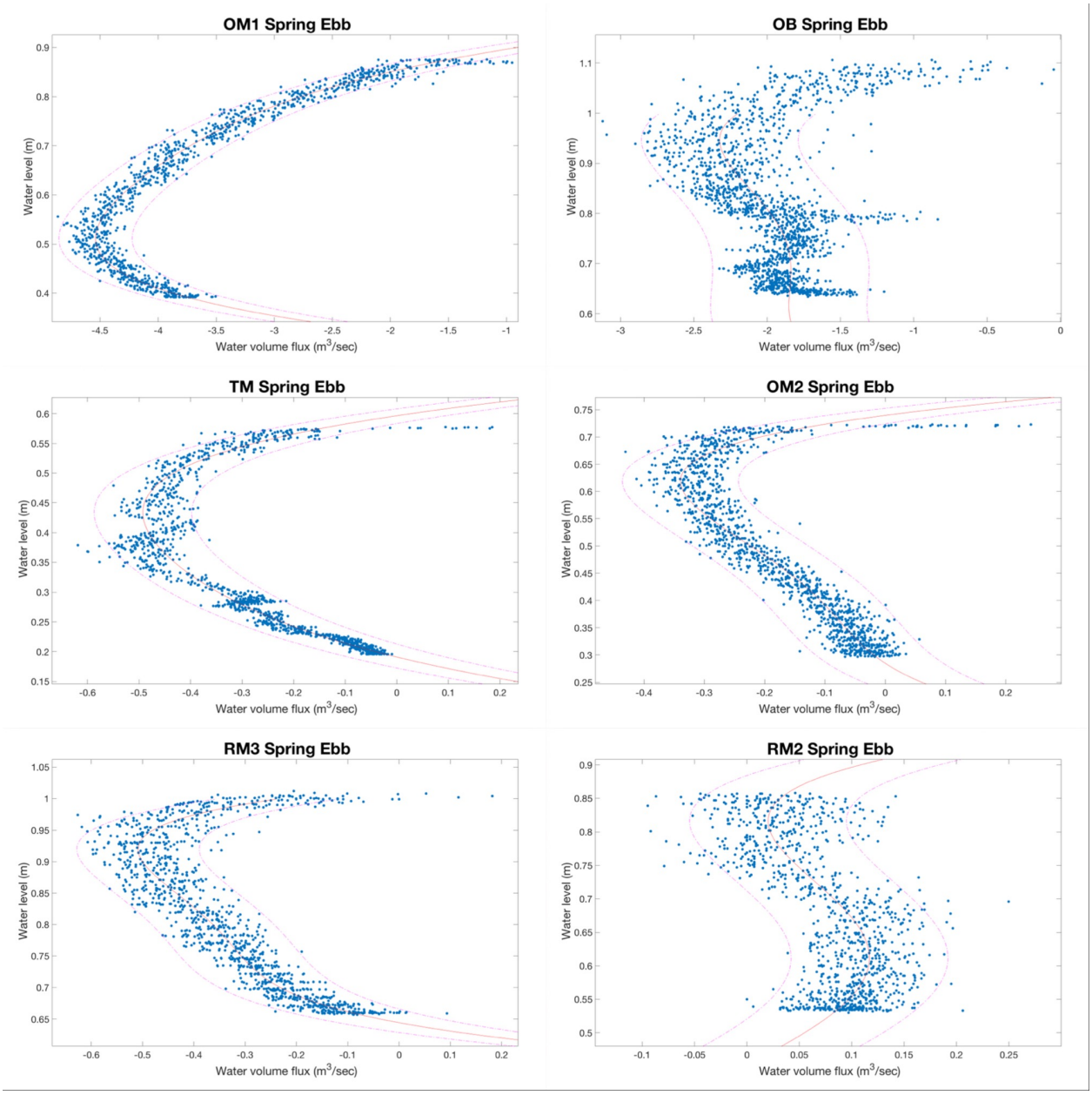

Figure 13. Site specific spring ebb rating curves post-restoration
Water volume flux (m^3 s^{-1}) relative to the water level (m) for all 6 makāha during spring ebb tide. A positive water volume flux represents flux into the fishpond from Kane‘ohe Bay or He‘eia Stream. A negative water volume flux represents flux out of the fishpond into Kane‘ohe Bay. Note the different flux (m^3 s^{-1}) scales on the x-axes.

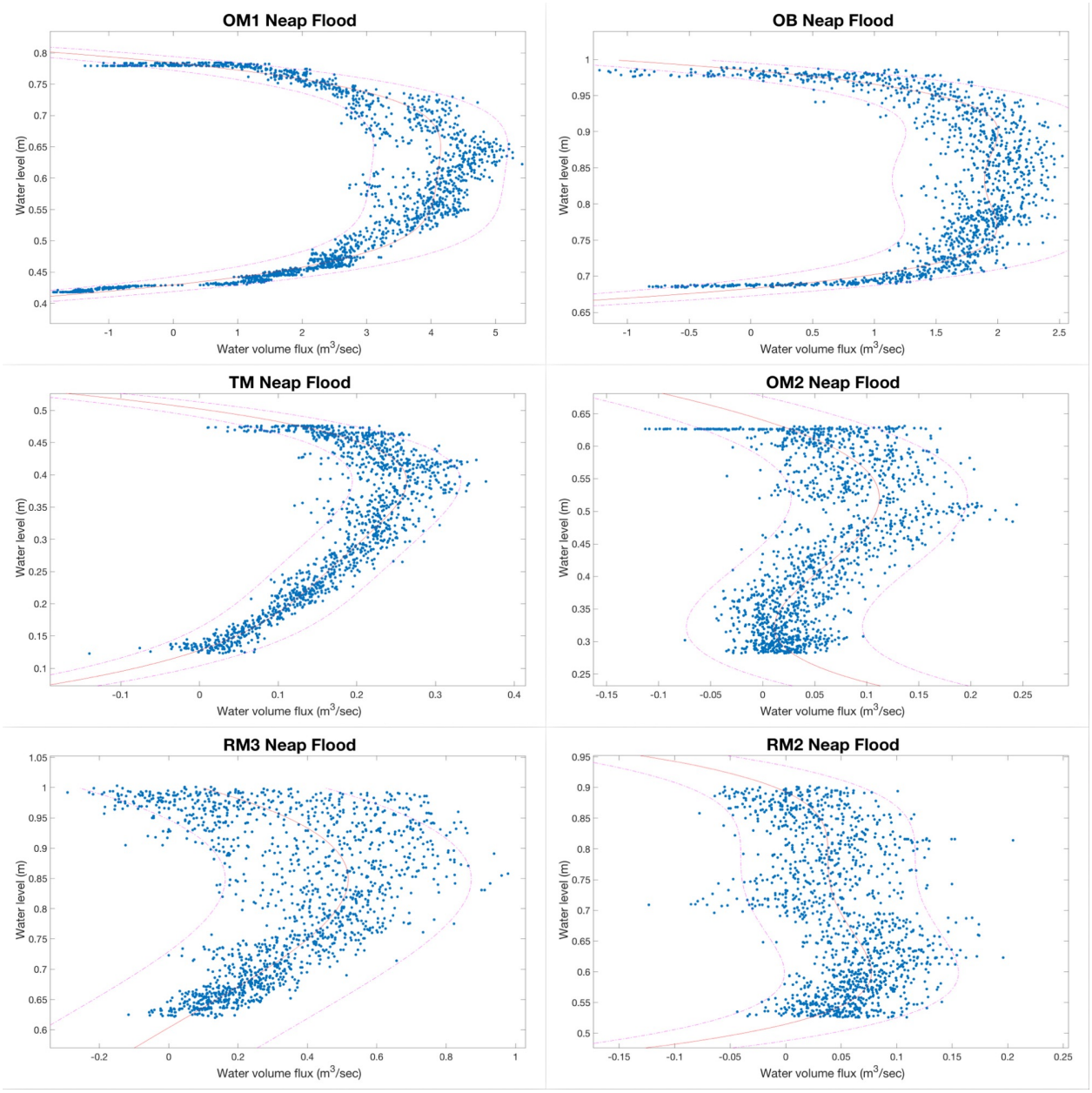

Figure 14. Site specific neap flood rating curves post-restoration
Water volume flux (m^3 s^{-1}) relative to the water level (m) for all 6 makāha during neap flood tide. A positive water volume flux represents flux into the fishpond from Kane‘ohe Bay or He‘eia Stream. A negative water volume flux represents flux out of the fishpond into Kane‘ohe Bay. Note the different flux (m^3 s^{-1}) scales on the x-axes.

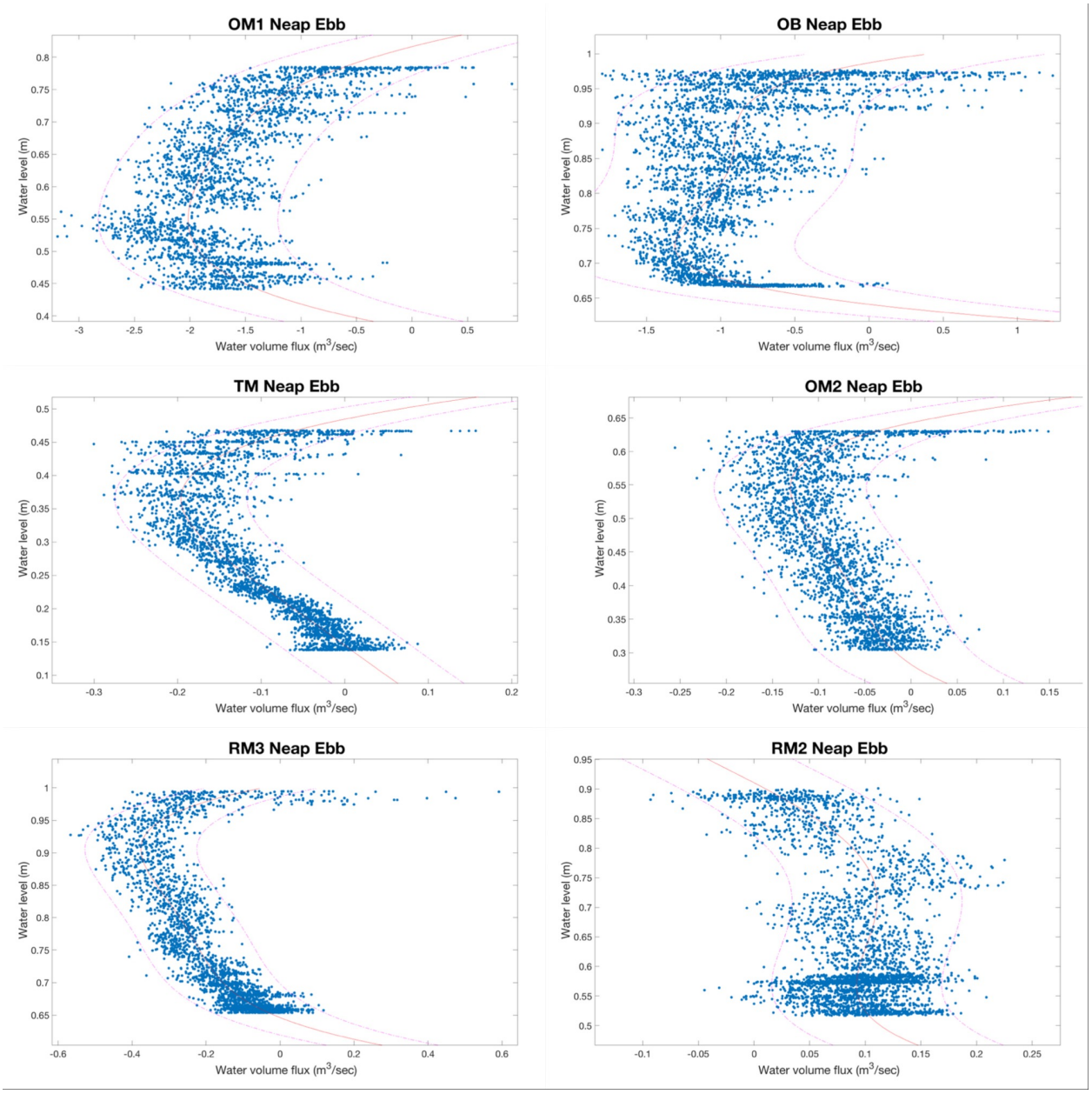

Figure 15. Site specific neap ebb rating curves post-restoration
Water volume flux (m^3 s^{-1}) relative to the water level (m) for all 6 mākāha during neap ebb tide. A positive water volume flux represents flux into the fishpond from Kāneʻohe Bay or Heʻeia Stream. A negative water volume flux represents flux out of the fishpond into Kāneʻohe Bay. Note the different flux (m^3 s^{-1}) scales on the x-axes.

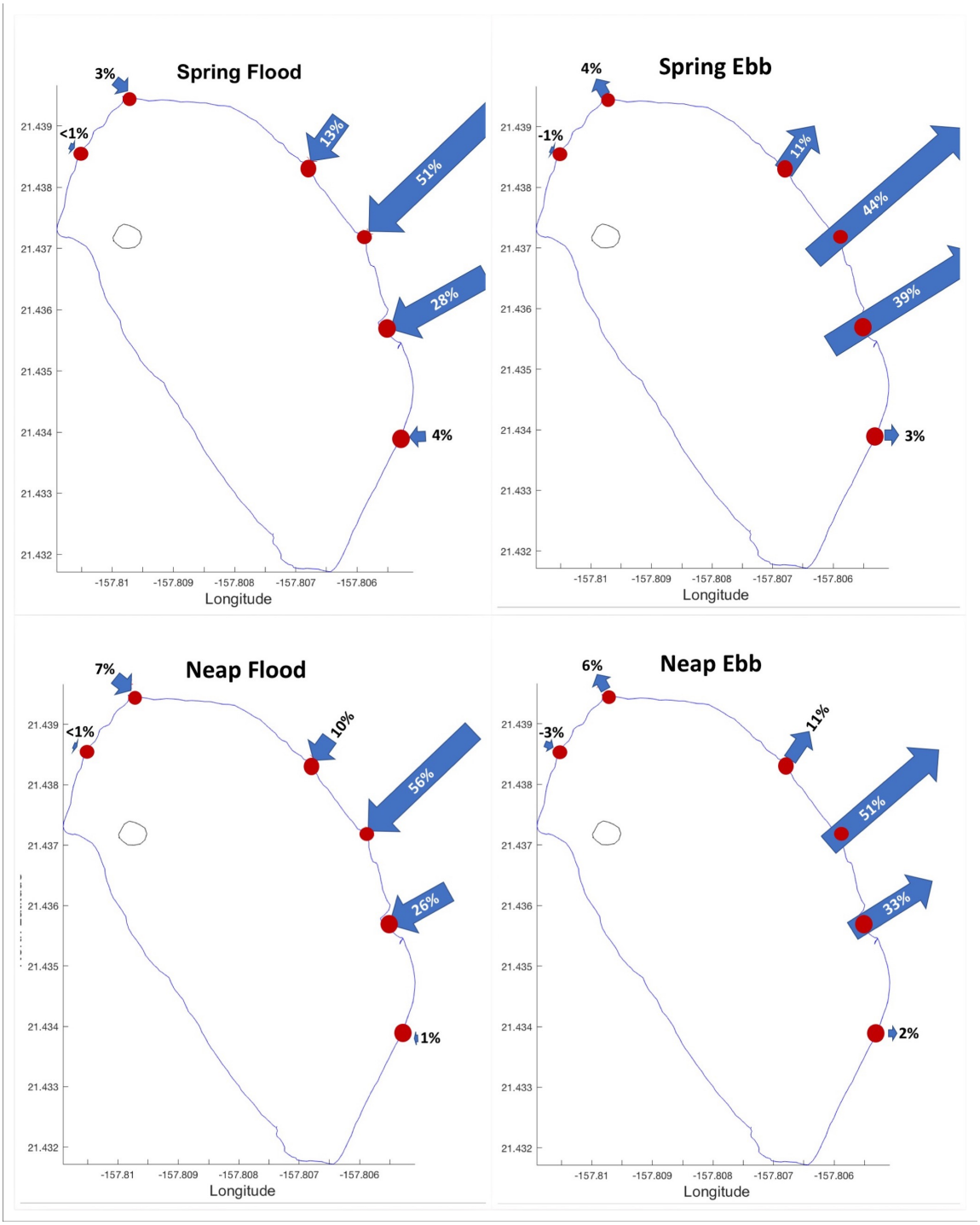

Figure 16. Mākāhā relative water flux comparison
Top left: Relative water flow through each mākāhā during a spring flood tide. Top right: Relative water flow through each mākāhā during a spring ebb tide. Bottom left: Relative water flow through each mākāhā during a neap flood tide. Bottom right: Relative water flow through each mākāhā during a neap ebb tide. Arrow length is a visual representation of relative magnitude of water flux at each mākāhā, normalized to the total flux for each respective cycle (outlined in Table 12). Filled red circles indicate locations of mākāhā.

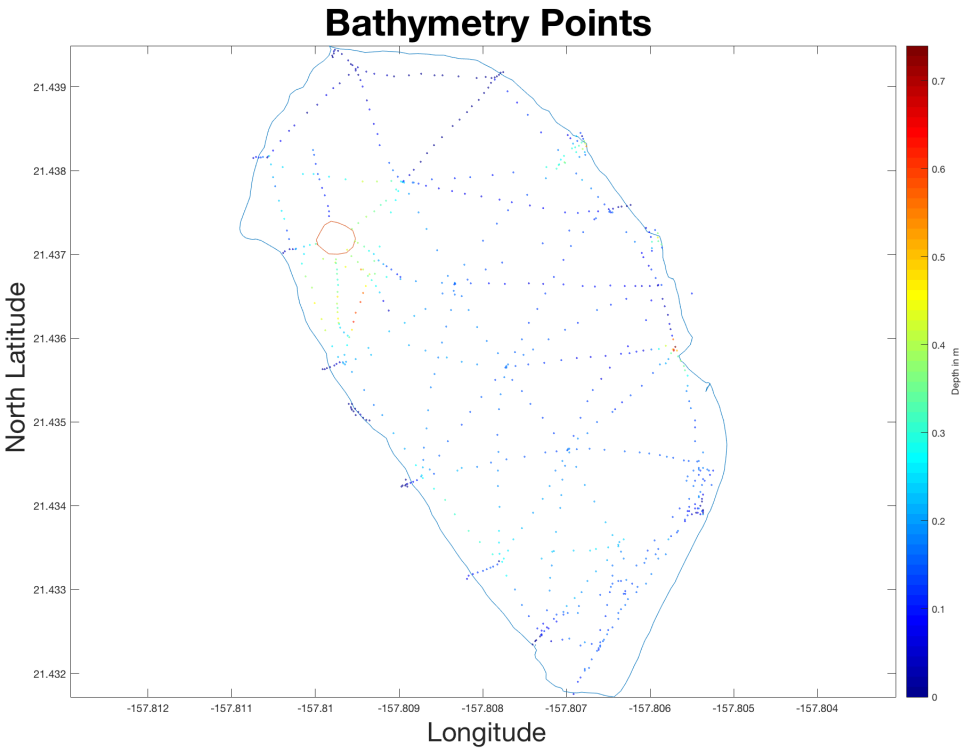

Figure 17. Bathymetry measurement points
A total of 728 waypoints were taken over a 10-day period in 2007. Depth was measured at each waypoint by manually submerging a depth-marked pole.

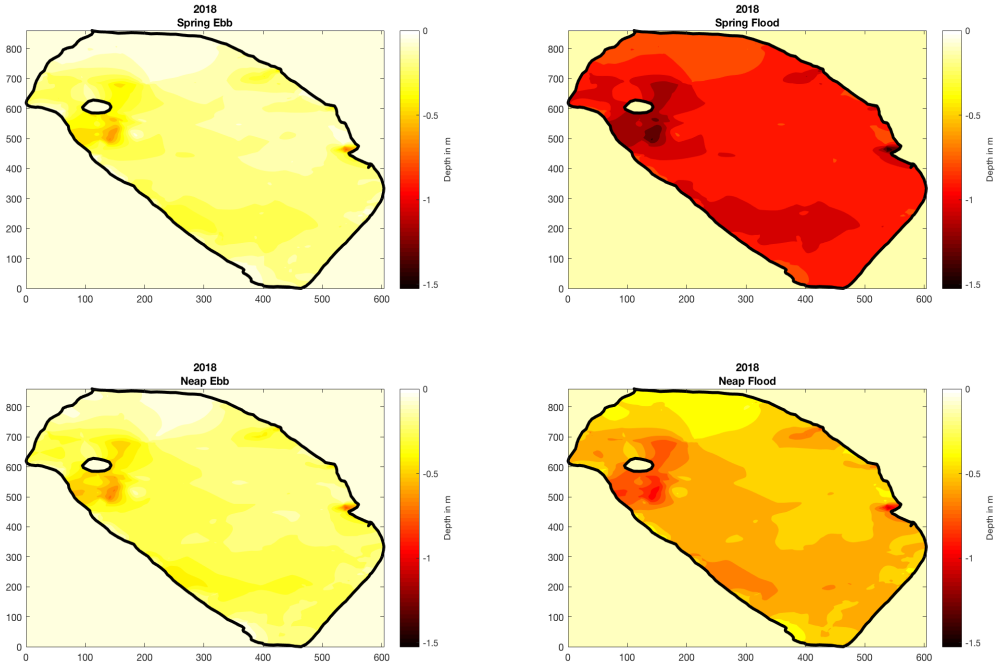

Figure 18. Post-restoration fishpond water level according to tidal state
Post-restoration fishpond water depth (in m) normalized to four tidal states: Spring ebb, spring flood, neap ebb and neap flood tide.

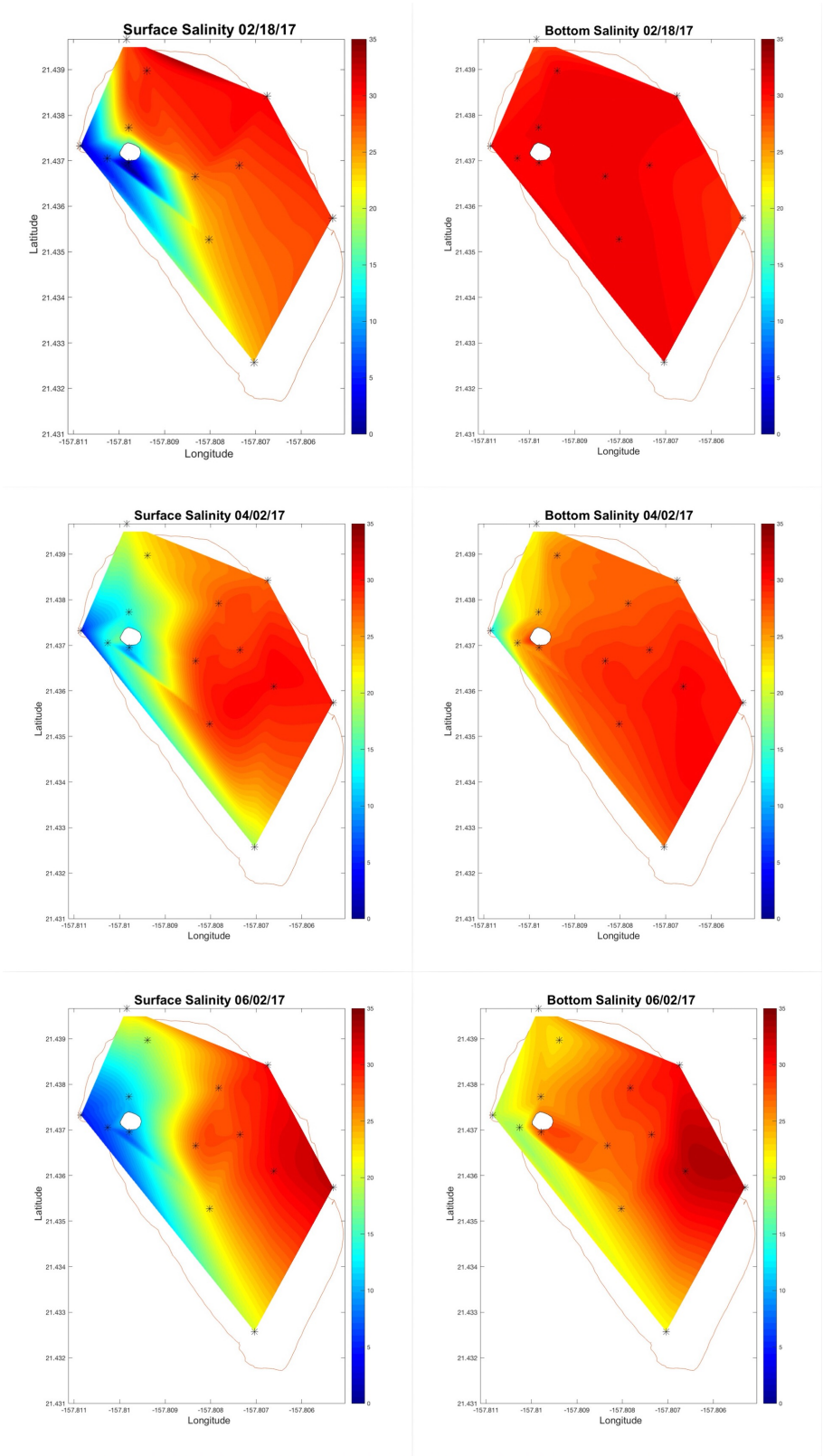

Figure 19. Spatial salinity distribution post-restoration
Surface and bottom spatial salinity distribution for three sampling events post-restoration.

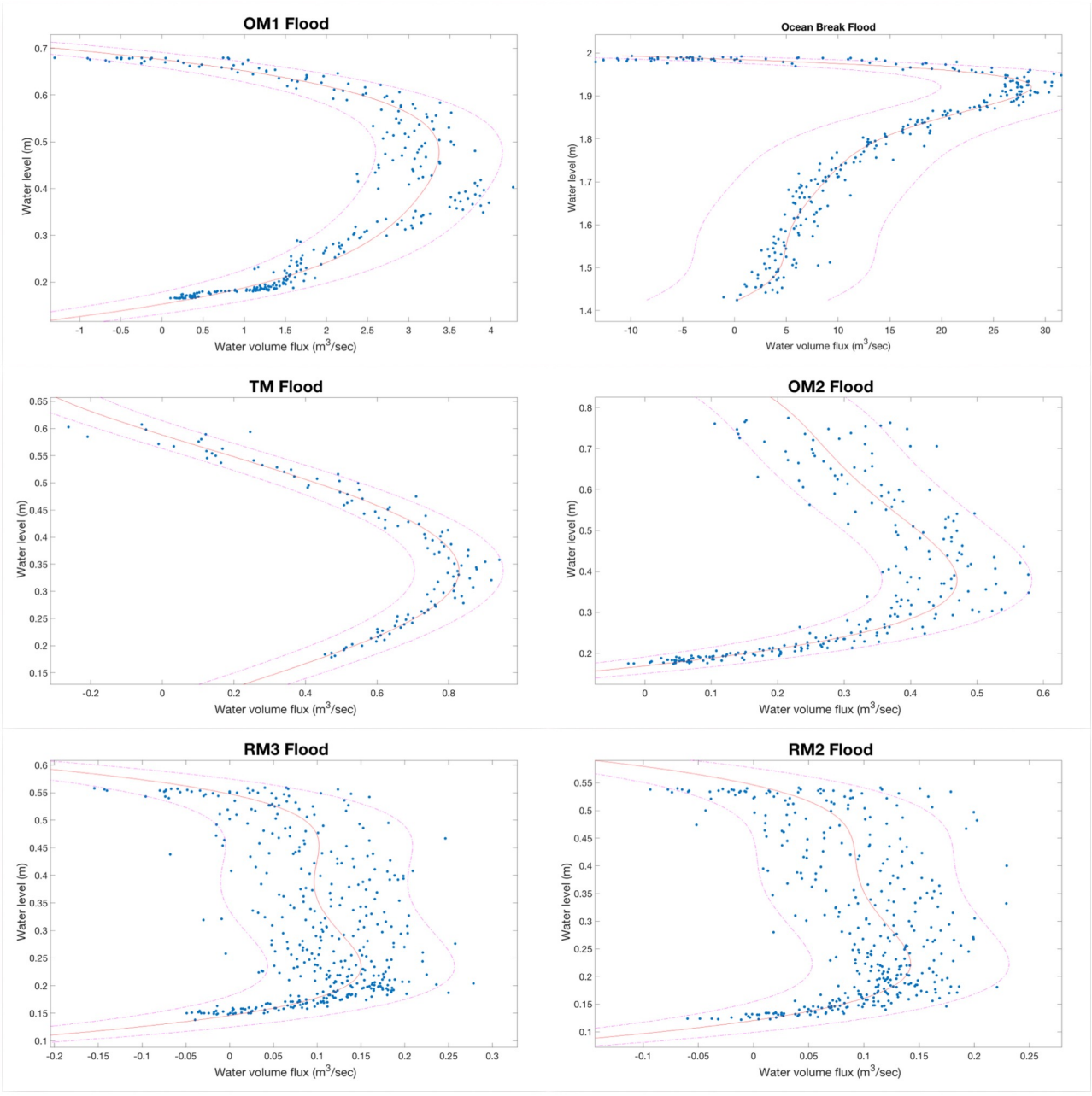

Figure 20. Site specific flood rating curves pre-restoration
Water volume flux (m^3 s^{-1}) relative to the water level (m) for all 6 mākāha during spring flood (OM1, OM2, OB, TM) and neap flood tide (RM2, RM3). A positive water volume flux represents flux into the fishpond from Kāneʻohe Bay or Heʻeia Stream. A negative water volume flux represents flux out of the fishpond into Kāneʻohe Bay. Note the different flux (m^3 s^{-1}) scales on the x-axes.

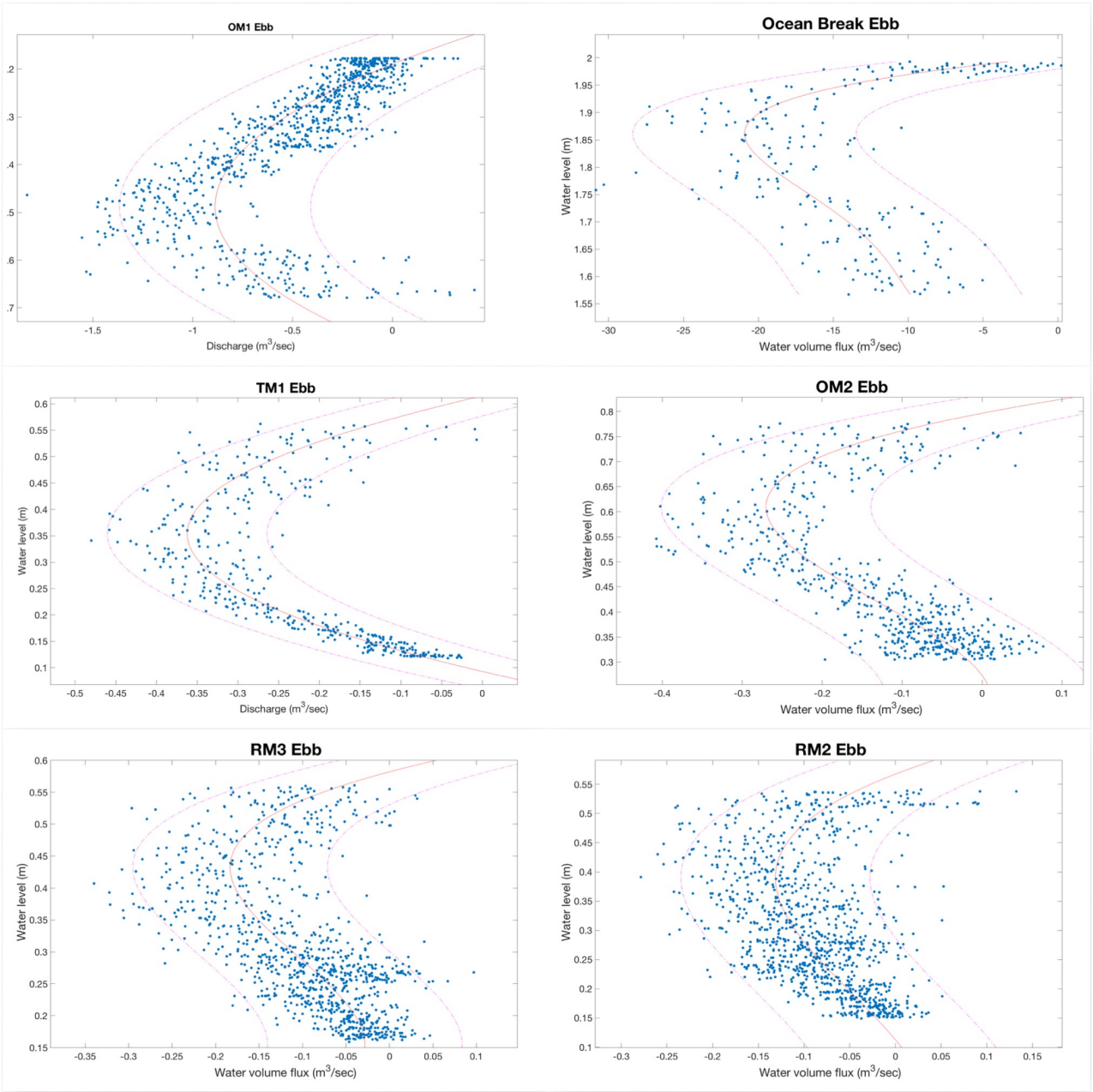

Figure 21. Site specific ebb rating curves pre-restoration
Water volume flux (m^3 s^{-1}) relative to the water level (m) for all 6 mākāha during spring ebb (OM1, OM2, OB, TM) and neap ebb tide (RM2, RM3). A positive water volume flux represents flux into the fishpond from Kāneʻohe Bay or Heʻeia Stream. A negative water volume flux represents flux out of the fishpond into Kāneʻohe Bay. Note the different flux (m^3 s^{-1}) scales on the x-axes.

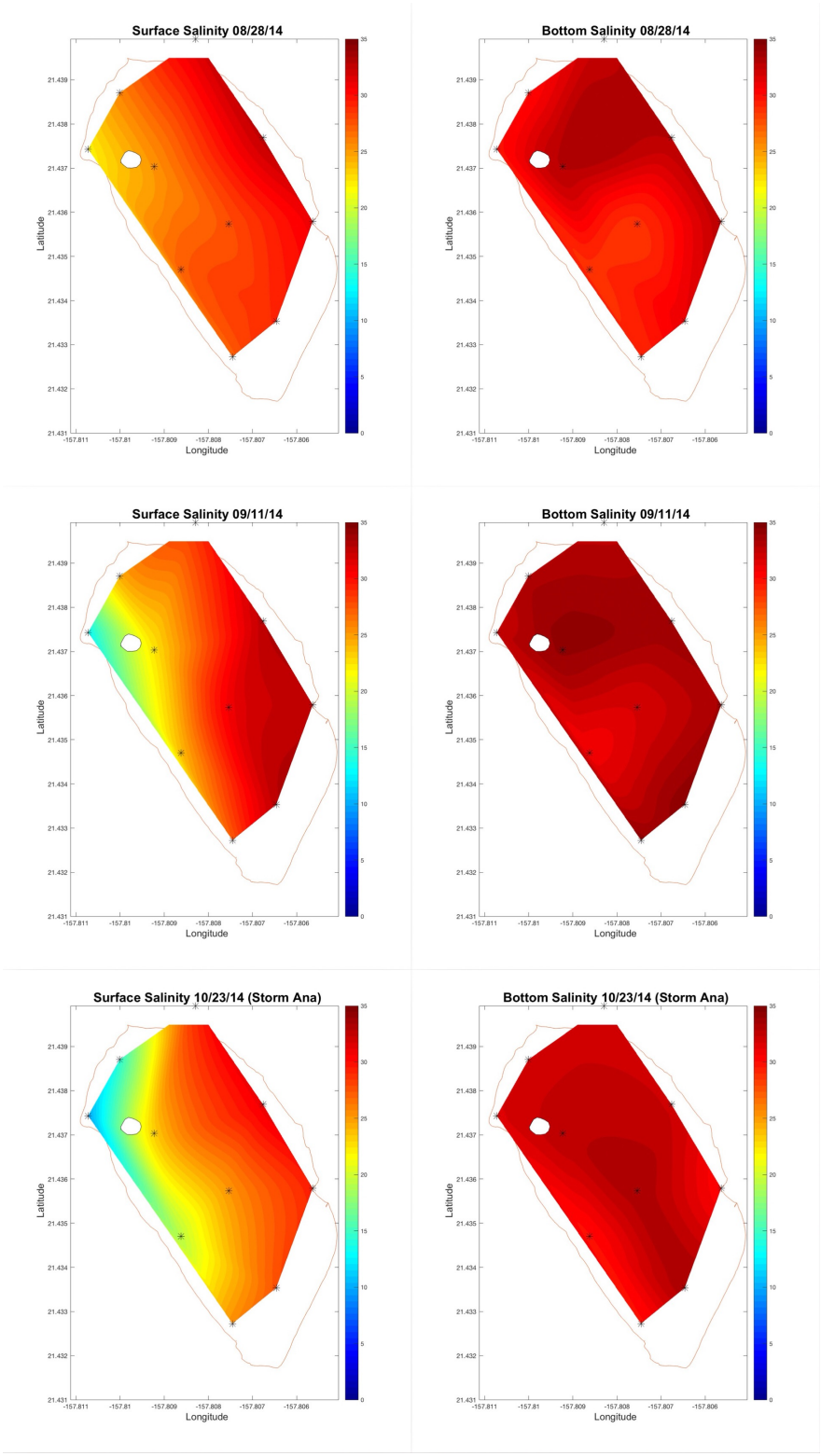

Figure 22. Spatial salinity distribution pre-restoration
Surface and bottom spatial salinity distribution for three sampling events pre-restoration.

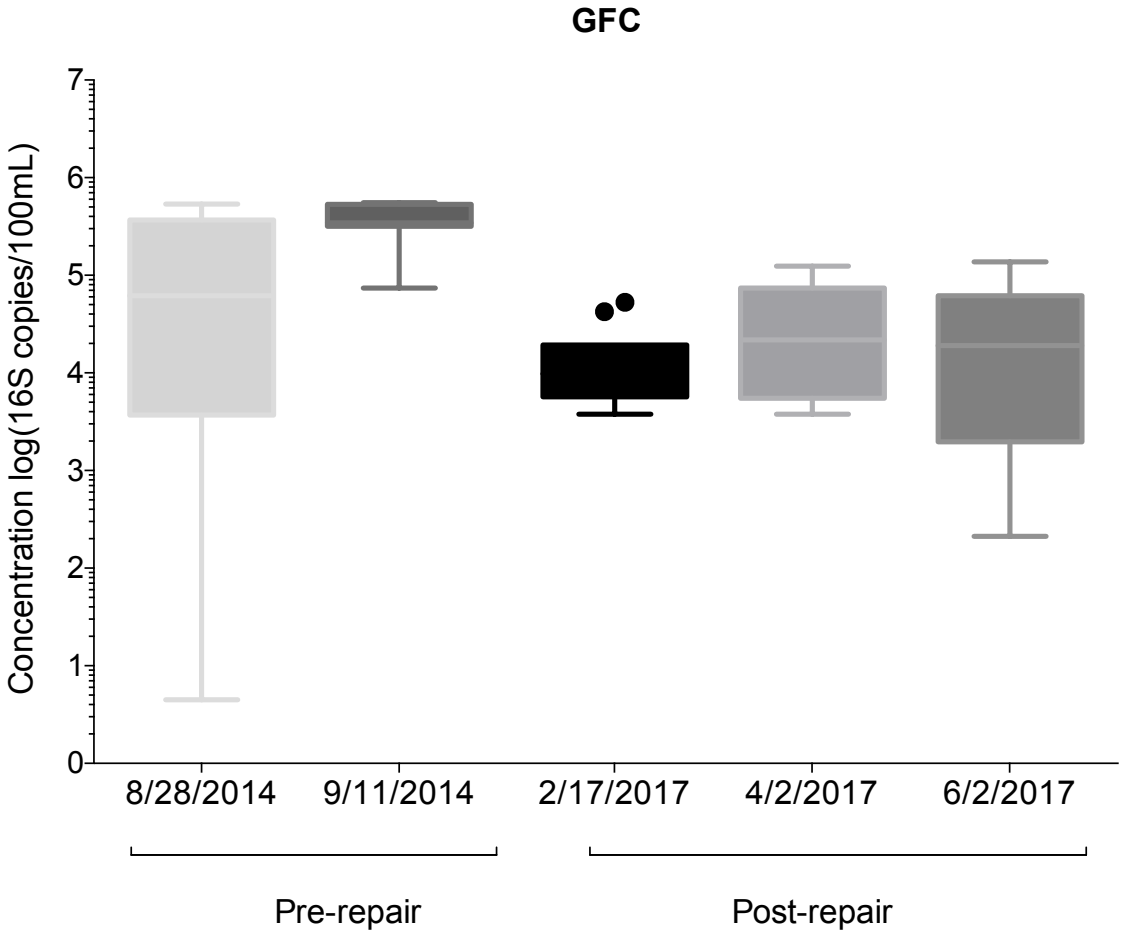

Figure 23. Bird specific *Fusobacteria* abundance pre- and post-restoration
Box plots with average GFC abundance across sampling locations, 95% confidence intervals and outliers for two sampling events pre-restoration and three sampling events post-restoration.

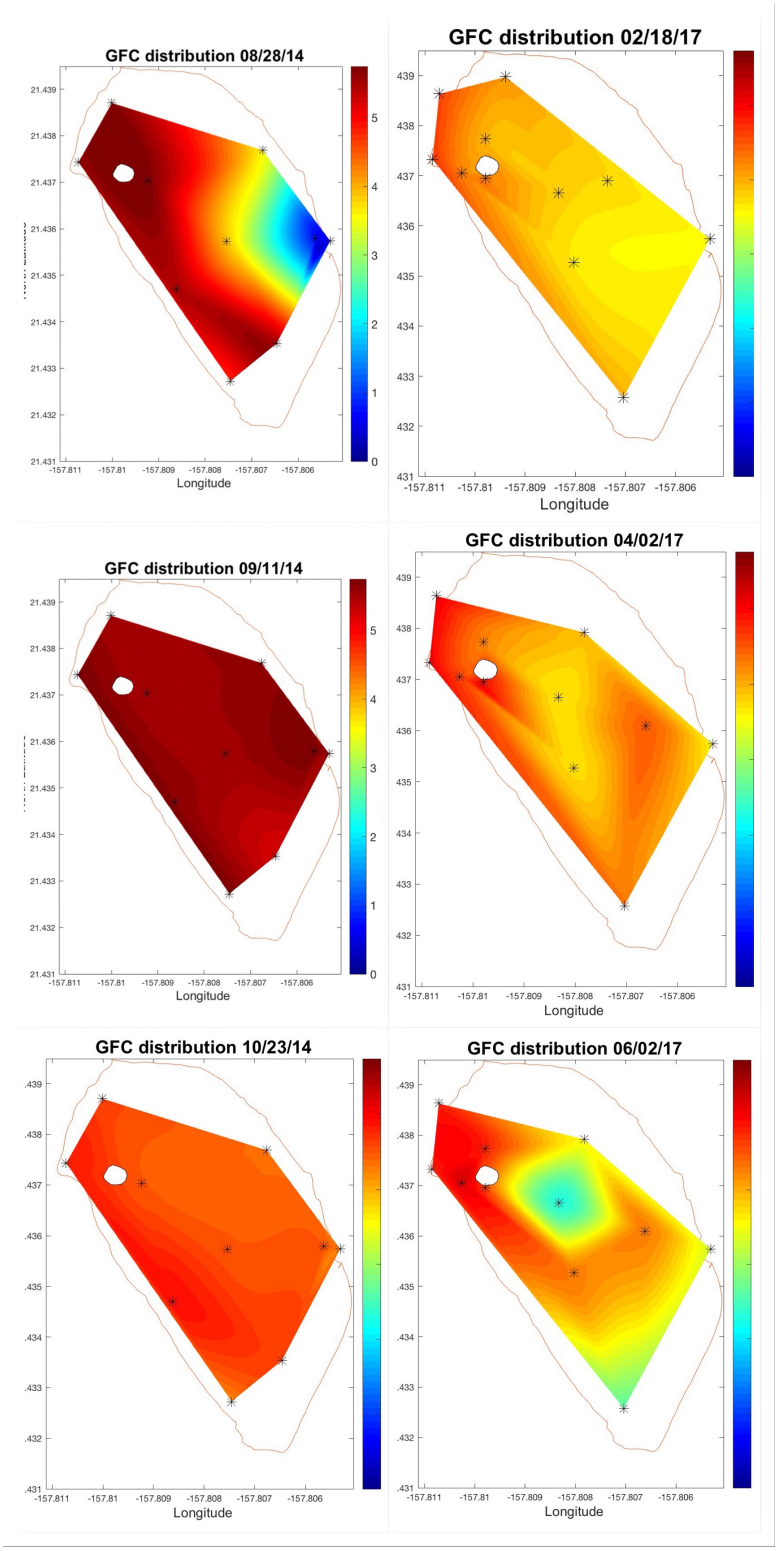

Figure 24. Spatial distribution of *Fusobacteria* abundance pre -and post-restoration
Spatial distribution of GFC abundance for three sampling events pre-restoration (left) and three sampling events post-restoration (right). Note that one storm event is included (10/23/2014).

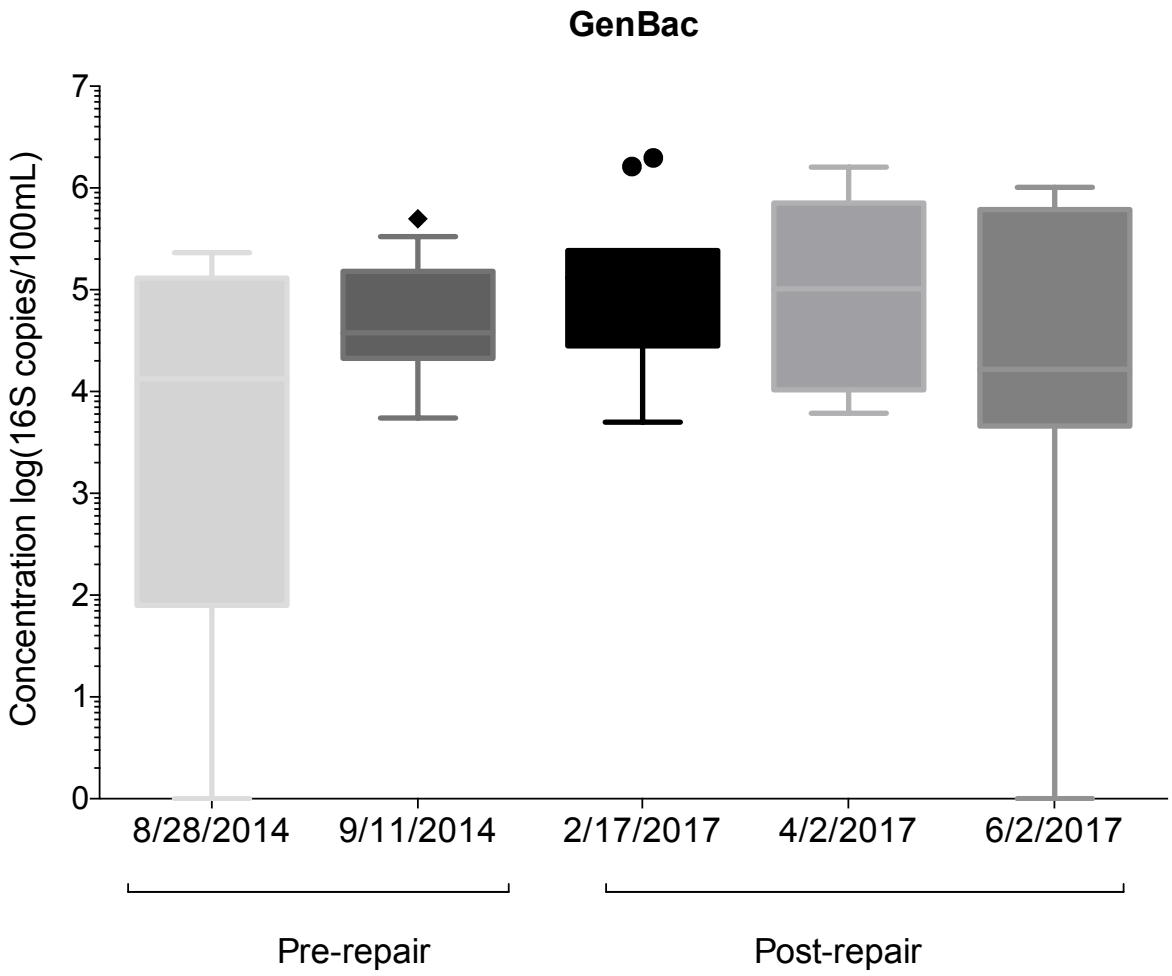

Figure 25. *Bacteroidales* abundance pre- and post-restoration
Box plots with average GenBac3 abundance across sampling locations, 95% confidence intervals and outliers for two sampling events pre-restoration and three sampling events post-restoration.

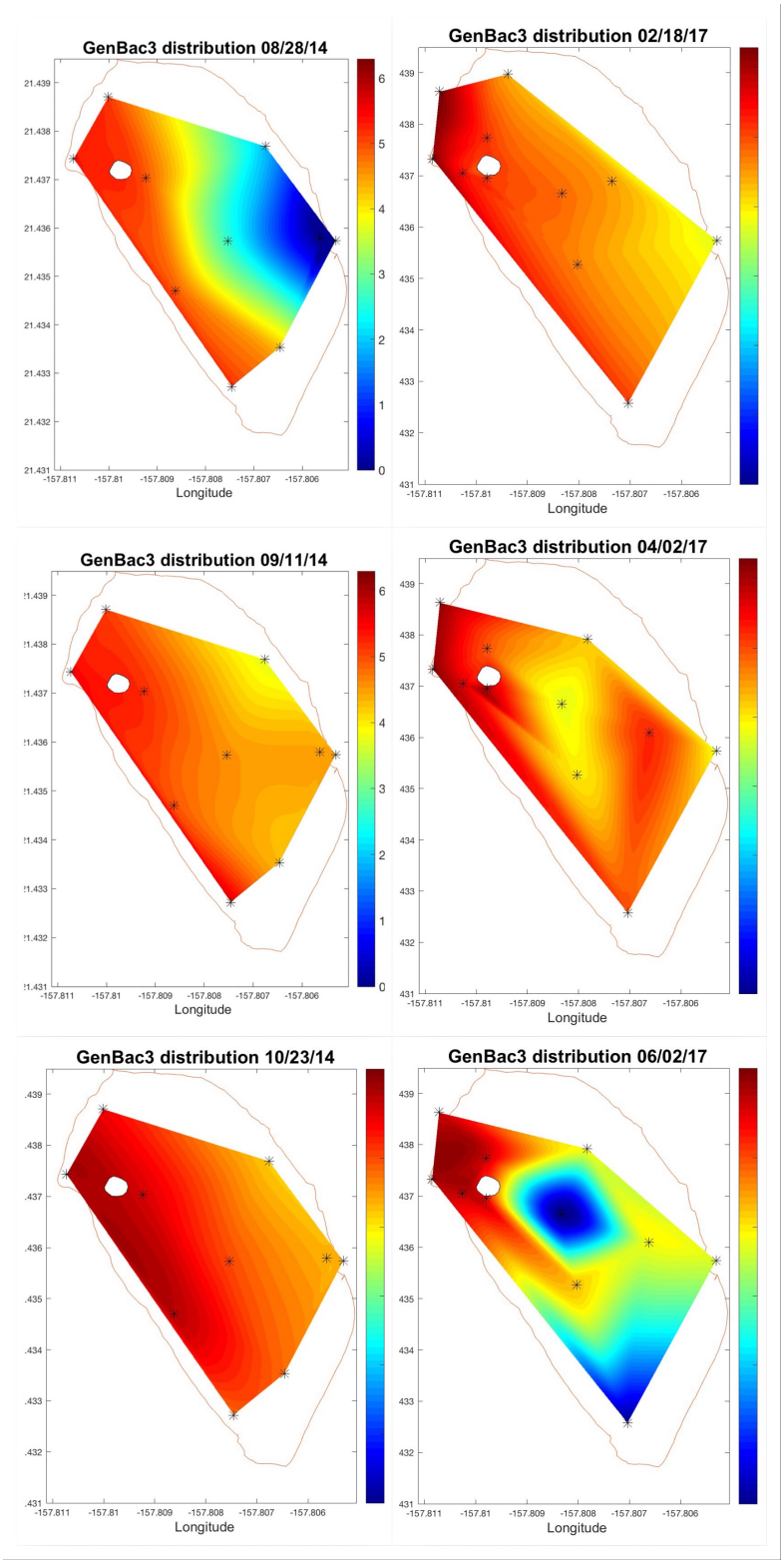

Figure 26. Spatial distribution of *Bacteroidales* abundance pre- and post-restoration
Spatial distribution of GenBac3 abundance for three sampling events pre-restoration (left) and three sampling events post-restoration (right). Note that one storm event is included (10/23/2014).

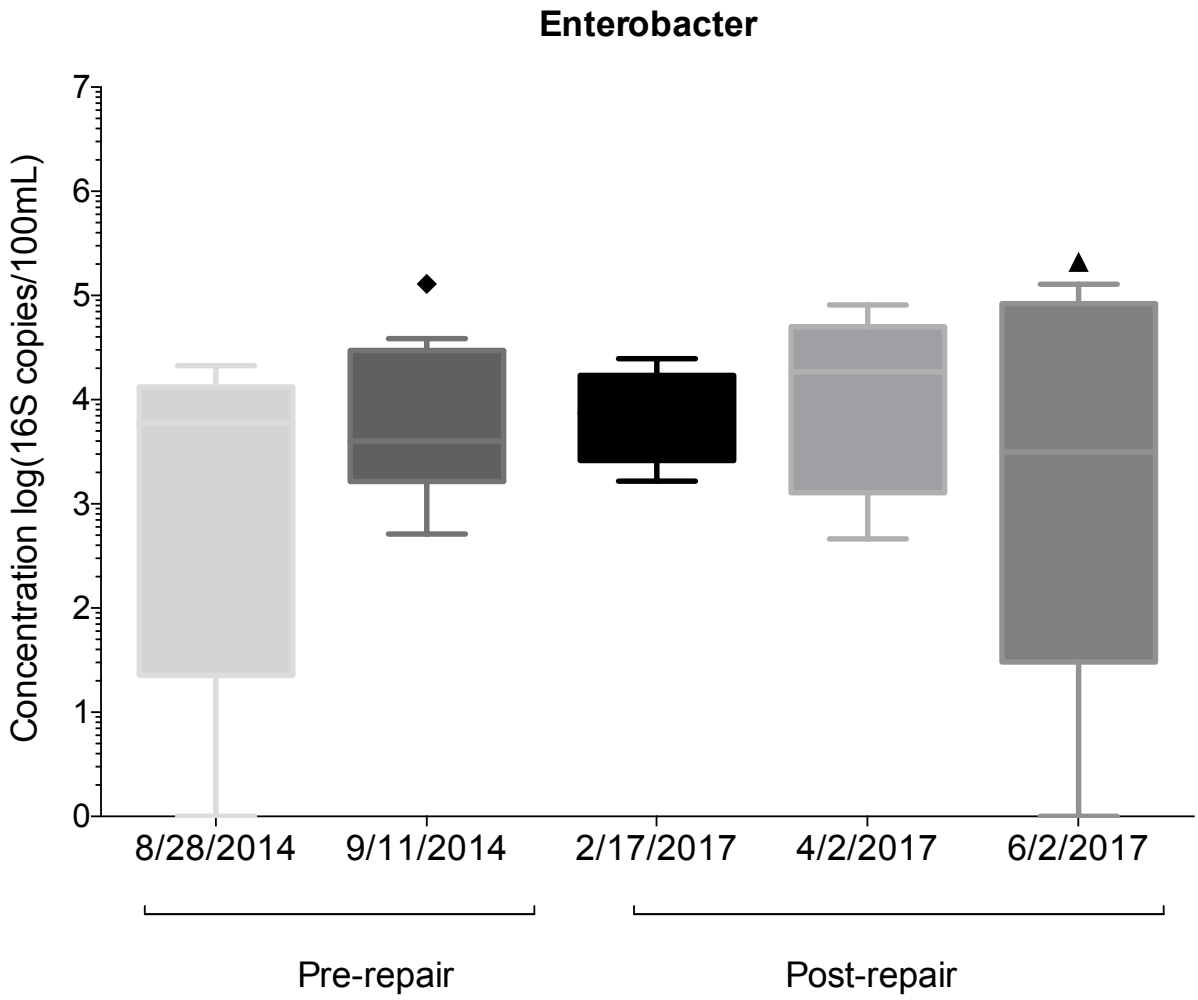

Figure 27. Enterococcus abundance pre- and post-restoration
Box plots with average Entero1a abundance across sampling locations, 95% confidence intervals and outliers for two sampling events pre-restoration and three sampling events post-restoration.

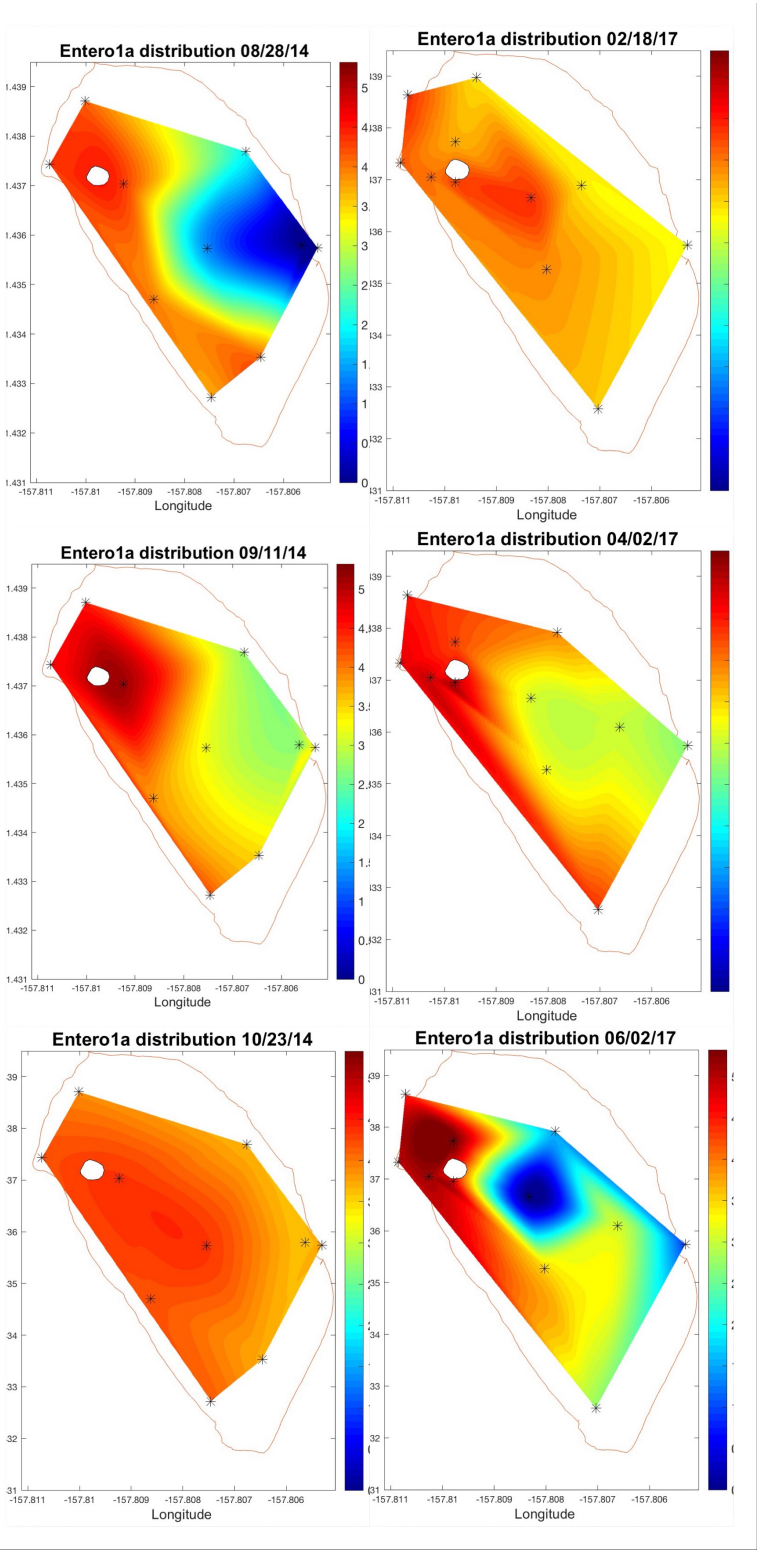

Figure 28. Spatial distribution of Enterococcus abundance pre- and post-restoration Spatial distribution of Entero1a abundance for three sampling events pre-restoration (left) and three sampling events post-restoration (right). Note that one storm event is included (10/23/2014).